

KEEPLoRA: CONTINUAL LEARNING WITH RESIDUAL GRADIENT ADAPTATION

Mao-Lin Luo^{1,2}, Zi-Hao Zhou^{1,2}, Yi-Lin Zhang^{1,2}, Yuanyu Wan³, Min-Ling Zhang^{1,2}, Tong Wei^{1,2†}

¹School of Computer Science and Engineering, Southeast University, Nanjing 210096, China

²Key Laboratory of Computer Network and Information Integration (Southeast University), Ministry of Education, China

³School of Software Technology, Zhejiang University, Ningbo, China

ABSTRACT

Continual learning for pre-trained vision-language models requires balancing three competing objectives: retaining pre-trained knowledge, preserving knowledge from a sequence of learned tasks, and maintaining the plasticity to acquire new knowledge. This paper presents a simple but effective approach called *KeepLoRA* to effectively balance these objectives. We first analyze the knowledge retention mechanism within the model parameter space and find that general knowledge is mainly encoded in the *principal* subspace, while task-specific knowledge is encoded in the *residual* subspace. Motivated by this finding, *KeepLoRA* learns new tasks by restricting LoRA parameter updates in the residual subspace to prevent interfering with previously learned capabilities. Specifically, we infuse knowledge for a new task by projecting its gradient onto a subspace orthogonal to both the principal subspace of pre-trained model and the dominant directions of previous task features. Our theoretical and empirical analyses confirm that *KeepLoRA* balances these three objectives and achieves state-of-the-art performance. The implementation code is available at <https://github.com/MaolinLuo/KeepLoRA>.

1 INTRODUCTION

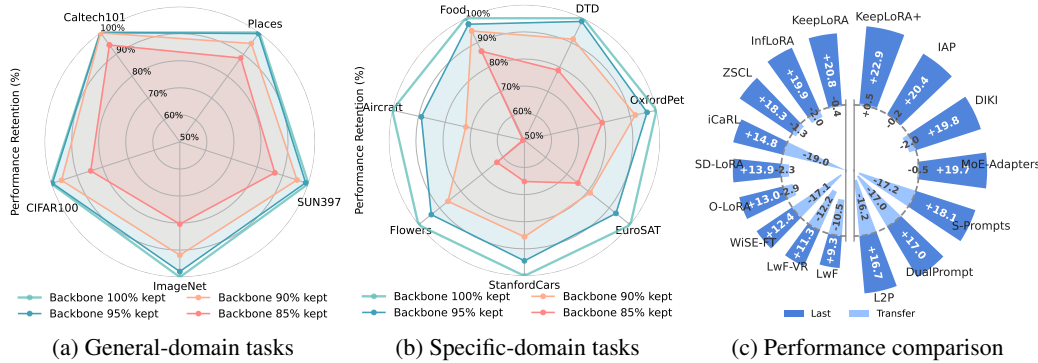


Figure 1: Analysis of model parameter subspaces and overall CL performance. In Fig. 1a and 1b, we measure zero-shot performance after reconstructing attention weights using only the top principal singular components. While performance on general-domain datasets remains highly robust, performance on most specific-domain datasets degrades sharply as more low-energy components are removed. In Fig. 1c, the *Last* metric measures the accuracy gain on the final learned task relative to a zero-shot baseline, while *Transfer* measures the accuracy degradation on unseen tasks.

[†]Corresponding author.

Table 1: Comparison of LoRA-based approaches to continual learning. When learning the t -th task, O-LoRA regularizes the down-projection matrix to be orthogonal to that of previous tasks to improve **stability**; InfLoRA constrains the optimization of task features \mathbf{H}_t to be orthogonal to previous dominant directions \mathbf{M}_{t-1} to jointly improve **plasticity** and stability; SD-LoRA optimizes a decoupled LoRA to improve stability and re-scales the magnitudes $\{\alpha_i\}_{i=1}^{t-1}$ of parameters from previous tasks to improve plasticity. By contrast, our method constrains optimization to a subspace orthogonal to both the principal weight subspace \mathbf{W}_p and previous task directions \mathbf{M}_{t-1} to preserve stability, and initializes the update in an optimal gradient space derived from \mathbf{G}_t to boost plasticity.

| Method | Initialization | | Training Objective |
|-----------------------------|--|--|--|
| | LoRA \mathbf{A} | LoRA \mathbf{B} | |
| O-LoRA (Wang et al., 2023a) | $\mathbf{A} \leftarrow \mathcal{N}(0, \sigma^2)$ | $\mathbf{B} \leftarrow \mathbf{0}$ | $\mathcal{L}_{\text{cls}}(\mathbf{A}_t, \mathbf{B}_t) + \sum_{i=0}^{t-1} \ \mathbf{A}_t^\top \mathbf{A}_i\ _F^2$ |
| InfLoRA (Liang & Li, 2024) | $\mathbf{USV}^\top = \text{SVD}(\mathbf{H}_t - \mathbf{M}_{t-1} \mathbf{M}_{t-1}^\top \mathbf{H}_t)$ $\mathbf{A} \leftarrow \mathbf{U}_r$ | $\mathbf{B} \leftarrow \mathbf{0}$ | $\mathcal{L}_{\text{cls}}(\mathbf{B}_t)$ |
| SD-LoRA (Wu et al., 2025b) | $\mathbf{A} \leftarrow \mathcal{N}(0, \sigma^2)$ | $\mathbf{B} \leftarrow \mathbf{0}$ | $\mathcal{L}_{\text{cls}}(\{\alpha_i\}_{i=1}^{t-1}, \alpha_t \mathbf{A}_t \mathbf{B}_t)$ |
| KeepLoRA (This paper) | $\text{SVD}(\mathbf{G}_t - \mathbf{W}_p \mathbf{W}_p^\top \mathbf{G}_t - \mathbf{M}_{t-1} \mathbf{M}_{t-1}^\top \mathbf{G}_t)$ $\mathbf{A} \leftarrow \mathbf{U}_r$ | $\mathbf{B} \leftarrow \mathbf{S}_r \mathbf{V}_r^\top$ | $\mathcal{L}_{\text{cls}}(\mathbf{B}_t)$ |

Vision-language models (VLMs) have demonstrated remarkable zero-shot transfer capabilities, making them cornerstones of many downstream applications (Comanici et al., 2025; Achiam et al., 2023; Radford et al., 2021). Despite this success, their performance on certain datasets can be insufficient, motivating the need for continual learning (CL). An effective CL method requires balance of three competing objectives: maintaining the ability to learn new knowledge (*plasticity*), preventing the forgetting of previously learned tasks (*backward stability*), and crucially, preserving the general pre-trained knowledge that guarantees general transferability (*forward stability*) (Mukhoti et al., 2024; Zheng et al., 2023). Degradation of this pre-trained knowledge is particularly detrimental, as it erodes the core value of VLMs. Therefore, the central challenge is how to learn new knowledge effectively without undermining these critical stability constraints.

A straightforward solution, replaying pre-training data, is rarely viable due to prohibitive computational costs and the frequent unavailability of proprietary training corpora (Wang et al., 2024; Zhou et al., 2024; Rolnick et al., 2019). The current alternatives largely follow two paths. The first is (i) *reference-data regularization*, which uses reference data to anchor the model parameters and retain stability (Wu et al., 2025a; Zheng et al., 2023). However, the success of these approaches is highly sensitive to the choice of reference data with additional training costs (Luo et al., 2025; Zheng et al., 2023). The second path involves (ii) *architecture extension*, such as prompt-pool (Fu et al., 2025; Wang et al., 2022b) or MoE-adapters (Yu et al., 2024; Dou et al., 2024) while freezing the model backbone. Although effective in preventing forgetting, these modules increase inference costs (Nayak et al., 2025) and complicate the deployment (Cai et al., 2025; Zadouri et al., 2023). Since trained weights are compact representations of data (Deletang et al., 2024; Franceschelli et al., 2024), an ideal CL method should infuse new knowledge directly into the existing parameter space, leveraging its inherent redundancy rather than accumulating external modules (Sharma et al., 2024).

To identify where new knowledge can be infused without disrupting existing abilities, we analyze the parameter space of the backbone attention weights via singular value decomposition (SVD). As shown in Fig. 1a and 1b, our analysis reveals that the principal subspace, spanned by components with large singular values, predominantly encodes general knowledge, while the residual subspace, associated with small singular values, encodes domain-specific knowledge. This observation indicates that performance on specialized datasets is highly sensitive to alterations in the residual subspace, whereas general datasets remain robust to such changes. This insight forms the basis of our approach: to coherently achieve *forward stability*, *backward stability*, and *plasticity*, CL updates should be constrained to the residual subspace, enabling the acquisition of new domain-specific knowledge without affecting the principal subspace that encodes general knowledge.

We implement our subspace-constrained updates using low-rank adaptation, a parameter-efficient method whose updates can be merged into the original weights post-training, thus incurring no inference overhead. Existing low-rank CL methods, such as O-LoRA (Wang et al., 2023a), InfLoRA (Liang & Li, 2024), and SD-LoRA (Wu et al., 2025b), lack considering the transfer ability of pre-

trained model and update directions within suboptimal subspaces, which limit their plasticity and stability as shown in Tab. 1. To overcome this, we initialize the low-rank update using the gradient from the first training step. This ensures that the update direction closely approximates the full-parameter tuning gradient to boost plasticity. To keep stability, we explicitly project this update into the residual subspace of the pre-trained weights. This constrains learning to directions that do not interfere with the model’s core transferable knowledge. Building on this, we construct a unified principal subspace that stores both the principal subspace of the model parameters and the dominant feature directions of each learned task. The unified principal subspace, with a size not exceeding the square of the feature dimension, effectively preserves both pre-trained and newly acquired knowledge.

Our contributions are summarized as follows:

- We empirically analyze the parameter space of pre-trained models and find that general knowledge is primarily encoded in the parameter principal subspace, while domain-specific adaptations are better captured by the residual subspace.
- We propose *KeepLoRA*, a novel method that leverages residual subspace constraints for parameter updates, validated by theoretical analysis showing how it optimally balances plasticity and stability through orthogonal projections.
- Experiments on dual-encoder (CLIP) and encoder-decoder (LLaVA) models validate that *KeepLoRA* effectively balances the three core challenges of plasticity, backward stability, and forward stability, establishing new state-of-the-art results on benchmark datasets.

2 RELATED WORKS

In continual learning, forward stability is typically preserved using reference-data regularization and architecture extension techniques. In addition, gradient projection methods are commonly employed to address backward stability and plasticity. In this section, we review these lines of work.

Reference-Data Regularization. Continual learning on narrow task distributions can cause the model feature space to collapse, degrading its pre-trained zero-shot transfer capabilities (Zheng et al., 2023). Reference-data methods aim to counteract this by anchoring the model representations. ZSCL (Zheng et al., 2023) uses the ImageNet (Deng et al., 2009) and Conceptual Captions (Sharma et al., 2018) datasets as reference data, employing distillation to preserve the feature space structure. However, the effectiveness of this approach is sensitive to the choice of reference data and the teacher model, with performance degrading when fewer images or classes are used (Zheng et al., 2023). Yu et al. (2024) propose MoE-Adapters by training a selector on the TinyImageNet (Deng et al., 2009) dataset to identify out-of-distribution data, which is then processed by the original frozen model. Wu et al. (2025a) leverage the generative model Stable Diffusion (Rombach et al., 2022) to create synthetic reference data for distillation. These methods inherently increase computational overhead and depend on external reference data, limiting their practical feasibility.

Architecture Extension. Architecture extension methods freeze the pre-trained model and extend it with new parameters for each task. L2P (Wang et al., 2022c) selects the most relevant prompts from a prompt pool, while DualPrompt (Wang et al., 2022b) uses explicitly task-sharing and task-specific prompts. CODA-Prompt (Smith et al., 2023) proposes end-to-end prompt selection methods to increase plasticity. MoE-Adapters (Yu et al., 2024) inserts a mixture of adapters into the image encoder, activating a subset for each task. DIKI (Tang et al., 2024) calibrates knowledge integration by determining the likelihood that a test sample belongs to a learned task. IAP (Fu et al., 2025) introduces Instance-Aware Gated Prompting to further improve the effectiveness of prompt selection. However, these methods cannot entirely avoid parameter selection errors or suboptimal activation coefficients. Moreover, this approach of adding external parameters does not truly infuse new knowledge into the base model.

Gradient Projection. Gradient projection methods mitigate catastrophic forgetting by constraining parameter updates into specific subspaces, thereby preventing interference with previously acquired knowledge (Qiao et al., 2024). In the context of full fine-tuning, methods such as Gradient Projection Memory (GPM) (Saha et al., 2021) enforce orthogonality between the gradients of a new

task and a stored basis of principal gradient directions from previous tasks. To improve the efficiency of full fine-tuning, CoSo (Cheng et al., 2025) utilizes Task-Specific Subspace Estimation and updates an orthogonal basis matrix. This thought has also been adapted to parameter-efficient techniques. For example, O-LoRA (Wang et al., 2023a) constrains the LoRA subspaces of new tasks to be orthogonal to those of previous tasks, ensuring that learning occurs in novel directions. InfLoRA (Liang & Li, 2024) applies a constraint where the LoRA down-projection matrix \mathbf{A} is orthogonal to GPM (Saha et al., 2021) or DualGPM (Liang & Li, 2023) to prevent interference. However, these existing methods primarily focus on mitigating backward forgetting, the loss of knowledge from previously learned sequential tasks. They do not explicitly address or analyze the preservation of general pre-trained knowledge, which is crucial for maintaining the model’s general transferability and preventing forward forgetting.

3 METHOD

3.1 PRELIMINARY

Problem Formulation. We adopt the multi-domain task incremental learning (MTIL) setting (Zheng et al., 2023), where the model encounters a sequence of n tasks $\{\mathcal{T}^1, \mathcal{T}^2, \dots, \mathcal{T}^n\}$. Each task $\mathcal{T}^i = (\mathcal{D}^i, \mathcal{C}^i)$ for $i \in \{1, 2, \dots, n\}$ comprises a dataset \mathcal{D}^i and corresponding class vocabulary \mathcal{C}^i . The dataset $\mathcal{D}^i = \{(\mathbf{x}_j^i, y_j^i)\}_{j=1}^{N_i}$ contains N_i training examples, where each \mathbf{x}_j^i denotes an input image and y_j^i represents the corresponding one-hot encoded ground truth label. The class vocabulary $\mathcal{C}^i = \{c_j^i\}_{j=1}^{m_i}$ establishes the mapping between categorical labels and semantic class names, with m_i denoting the total number of distinct classes for task \mathcal{T}^i . During inference, the model classifies an input image \mathbf{x} within \mathcal{C}^i . The goal of continual learning is to maintain performance on pre-trained knowledge and all previously encountered tasks while adapting to new ones.

Vanilla LoRA. Low-rank adaptation (LoRA) (Hu et al., 2022) decomposes weight updates into two low-rank matrices $\mathbf{A} \in \mathbb{R}^{d_{\text{in}} \times r}$ and $\mathbf{B} \in \mathbb{R}^{r \times d_{\text{out}}}$, where $r \ll \min(d_{\text{in}}, d_{\text{out}})$. During training, \mathbf{W} remains frozen while only \mathbf{A} and \mathbf{B} are fine-tuned. The matrices are initialized with $\mathbf{A} \sim \mathcal{N}(0, \sigma^2)$ and $\mathbf{B} = \mathbf{0}$. For input $\mathbf{x} \in \mathbb{R}^{d_{\text{in}}}$, the forward pass becomes:

$$\mathbf{y} = \mathbf{x} \left(\mathbf{W} + \frac{\alpha}{r} \mathbf{A} \mathbf{B} \right) \quad (1)$$

where α is a scaling factor.

3.2 KEEPLORA: GRADIENT PROJECTION ADAPTATION

Continual learning for pre-trained vision-language models demands a balance between *plasticity*, the ability to acquire new knowledge, and *learning stability*, which comprises both *forward stability* to preserve general pre-trained knowledge and *backward stability* to retain knowledge from previously learned tasks. To address this problem, we propose *KeepLoRA*, a method built upon LoRA that employs residual subspace constraints to unify stability preservation and new knowledge infusion.

Stability: Preserving Pre-trained and Previous Task Knowledge. KeepLoRA retains stability by projecting the subspaces of pre-trained knowledge and previous task knowledge onto a unified principal subspace. Subsequent adaptations for new tasks are then confined to the residual subspace orthogonal to this principal subspace, thereby minimizing interference with the learned knowledge.

Pre-trained Knowledge Subspace: We analyze the parameters of the pre-trained model to understand how the model stores general knowledge. Specifically, we decompose each weight matrix $\mathbf{W} \in \mathbb{R}^{d_{\text{in}} \times d_{\text{out}}}$ requiring updates via singular value decomposition (SVD) as $\mathbf{W} = \mathbf{U} \mathbf{S} \mathbf{V}^\top$. The decomposition produces a subspace $\mathbf{W}_p = \mathbf{U}_{:,1:p}$, and the subspace is constrained such that:

$$\|\mathbf{W}_p\|_F^2 \geq \epsilon_w \|\mathbf{W}\|_F^2 \quad (2)$$

where $\epsilon_w \in (0, 1)$ controls the energy ratio retained in \mathbf{W}_p .

Previous Task Knowledge Subspace: To mitigate forgetting of learned tasks, the LoRA module updating matrix \mathbf{W} for new tasks should minimize interference with features from previous tasks. Specifically, our goal is to make $\mathbf{Y} = \text{LoRA}_t(\mathbf{X})$ as close to $\mathbf{0}$ as possible for any input \mathbf{X} from

previous tasks $\{\mathcal{T}_i\}_{i=1}^{t-1}$. Since no real or synthetic samples from previous tasks are available for replay, we propose to extract the dominant singular vectors of previous tasks as the dominant feature directions. This approach enables us to continuously compress task-specific information and enforce matrix \mathbf{A} to be orthogonal to the dominant singular vectors on LoRA initialization. After training for task t , we extract and store the dominant feature directions for this task. These directions are chosen to be orthogonal to the subspace jointly defined by the principal weights and the dominant feature directions of all $t-1$ tasks. We then define the feature space for the t -th task as:

$$\hat{\mathbf{X}}_t = \mathbf{X}_t - \mathbf{W}_p \mathbf{W}_p^\top \mathbf{X}_t - \mathbf{M}_{t-1} \mathbf{M}_{t-1}^\top \mathbf{X}_t \quad (3)$$

where $\mathbf{M}_{t-1} \in \mathbb{R}^{d_{in} \times k}$ represents the accumulated direction matrix containing the dominant singular vectors from tasks $\{1, 2, \dots, t-1\}$, and k denotes the total number of stored singular vectors. We initialize $\mathbf{M}_0 = \emptyset$ as an empty matrix. The number of stored vectors k is dynamically determined by an energy threshold $\epsilon_f \in (0, 1)$. Specifically, we retain the minimum number k of dominant directions required to satisfy:

$$\|\hat{\mathbf{X}}_t\|_F^2 + \|\mathbf{W}_p \mathbf{W}_p^\top \mathbf{X}_t\|_F^2 + \|\mathbf{M}_{t-1} \mathbf{M}_{t-1}^\top \mathbf{X}_t\|_F^2 \geq \epsilon_f \|\mathbf{X}_t\|_F^2 \quad (4)$$

We perform SVD on the features $\hat{\mathbf{X}}_t = \mathbf{U}_t \mathbf{S}_t \mathbf{V}_t^\top$ and extract the top- m dominant singular vectors to update our subspace matrix: $\mathbf{M}_t = [\mathbf{M}_{t-1}, \mathbf{V}_{t(:,1:m)}]$, where m is determined by a threshold ϵ_f .

Unified Principal Subspace. Since both \mathbf{W}_p and \mathbf{M}_t consist of orthogonal direction vectors operating within the same d_{in} -dimensional feature space, and the total number of orthogonal vectors is upper-bounded by d_{in} , we can mathematically unify them into a single projection subspace: $\mathbf{M}'_t = [\mathbf{W}_p, \mathbf{M}_t]$. The unified subspace leverages the theoretical foundation that predictive models can be transformed into lossless compressors (Deletang et al., 2024) and model weights embody a compressed representation of the training data (Franceschelli et al., 2024). Under this perspective, \mathbf{W}_p captures the essential feature representation space of the pre-training data, while \mathbf{M}_t preserves the dominant feature directions during continual learning. Both components represent compressed knowledge from their respective data distributions.

To ensure the new t -th task updates never interfere \mathbf{M}'_{t-1} , KeepLoRA achieves this through a modified LoRA approach, where matrix \mathbf{A} is initialized within $\{\mathbf{M}'_{t-1}\}^\perp$ and frozen throughout training, while only \mathbf{B} is optimized.

Plasticity: Gradient-Informed LoRA Initialization in Residual Subspace. While the unified principal subspace ensures learning stability, KeepLoRA also requires maintaining plasticity to adapt to new tasks. We achieve it by initializing the LoRA module using task-specific gradient information, aligning adaptation directions with full fine-tuning while confining updates to $\{\mathbf{M}'_{t-1}\}^\perp$. Specifically, we utilize gradient information to guide the initialization within the constrained residual space. Let $\mathbf{G}_t = \nabla_{\mathbf{W}} \mathcal{L}(\mathbf{W}; \mathcal{D}^t)$ denotes the gradient of the weight matrix \mathbf{W} of the t -th task at the first training step. We project this gradient onto the residual subspace:

$$\hat{\mathbf{G}}_t = \underbrace{\mathbf{G}_t}_{\text{plasticity}} - \underbrace{\mathbf{W}_p \mathbf{W}_p^\top \mathbf{G}_t - \mathbf{M}_{t-1} \mathbf{M}_{t-1}^\top \mathbf{G}_t}_{\text{forward and backward stability}} \quad (5)$$

We perform SVD on the projected gradient $\hat{\mathbf{G}} = \mathbf{U} \mathbf{S} \mathbf{V}^\top$ and initialize the LoRA matrices with top- r singular vectors as:

$$\mathbf{A} = \mathbf{U}_{:,1:r}, \quad \mathbf{B} = \mathbf{S}_{1:r} \mathbf{V}_{:,1:r}^\top \quad (6)$$

where $\mathbf{U}_{:,1:r}$ denotes the first r columns of \mathbf{U} , and r is the rank parameter. This gradient-informed initialization directly simulates the update direction of full fine-tuning while operating within the residual subspace, enabling effective adaptation without undermining these critical stability constraints. Since the initial product $\frac{\alpha}{r} \mathbf{A} \mathbf{B}$ is non-zero, the frozen parameter \mathbf{W} can be adjusted to maintain the initial parameter values unchanged. Specifically, we replace the original parameter \mathbf{W} with $\mathbf{W}' = \mathbf{W} - \frac{\alpha}{r} \mathbf{A} \mathbf{B}$ to ensure that the initial forward pass behavior remains identical with the initial model. Algorithm 1 summarizes the proposed KeepLoRA method.

3.3 DISCUSSION OF KEEPLORA

Eq. 5 and Eq. 6 serve as the core formulas of KeepLoRA, enabling its balance of plasticity and stability: \mathbf{G}_t enhances plasticity by identifying new task adaptation directions, while the subtracted terms

Algorithm 1 KeepLoRA for Continual Learning

```

1: Input: Pre-trained model  $f_\theta$  with updatable parameters  $\{\mathbf{B}_i\}$ , task sequence  $\{\mathcal{T}^t\}_{t=1}^n$ , hyper-
   parameters  $\epsilon_w, \epsilon_f, r, \alpha$ 
2: Output: Updated model  $f_\theta$  with merged LoRA adapters
3: for task  $t = 1$  to  $n$  do
4:   Initialize KeepLoRA through Eq. 5 and Eq. 6
5:   Replace the parameter  $\mathbf{W}$  with the modified frozen parameter  $\mathbf{W}' = \mathbf{W} - \frac{\alpha}{r} \mathbf{A}_t \mathbf{B}_t$ 
6:   Compute the loss and optimize the KeepLoRA parameters  $\mathbf{B}_t$ 
7:   Merge KeepLoRA and current model by  $\mathbf{W} = \mathbf{W}' + \frac{\alpha}{r} \mathbf{A}_t \mathbf{B}_t$ 
8:   Extract dominant feature directions through Eq. 3 and Eq. 4
9: end for

```

remove gradients that interfere with pre-trained and previous task knowledge, ensuring stability. To verify these core designs, we first establish the equivalence between KeepLoRA parameter update rule and gradient projection learning, defining the necessary properties of the subspace spanned by \mathbf{A}_t . We then demonstrate that the initialization of \mathbf{A}_t meets these properties.

Analyzes of Frozen \mathbf{A}_t LoRA Updates. The KeepLoRA parameter update method involves freezing \mathbf{A}_t and optimizing only \mathbf{B}_t . The following proposition demonstrates that this update rule is equivalent to gradient descent constrained within the subspace $\text{span}(\mathbf{A}_t)$.

Proposition 3.1. *(LoRA with frozen down-projection \mathbf{A}_t is equivalent to gradient projection update.) Let $\mathcal{L}(\mathbf{W}; \mathcal{D}^t)$ denote the loss function for the t -th task \mathcal{T}^t , where: $\mathbf{W} = \mathbf{W}' + \frac{\alpha}{r} \mathbf{A}_t \mathbf{B}_t$, $\mathbf{G}_t = \nabla_{\mathbf{W}} \mathcal{L}(\mathbf{W}; \mathcal{D}^t)$. Optimizing only \mathbf{B}_t through gradient descent with learning rate η is equivalent to performing gradient descent on the orthogonal projection of \mathbf{G}_t onto $\text{span}(\mathbf{A}_t)$. The weight update of \mathbf{W} satisfies:*

$$\Delta \mathbf{W} = \frac{\alpha}{r} \mathbf{A}_t \Delta \mathbf{B}_t = -c \mathbf{A}_t \mathbf{A}_t^\top \mathbf{G}_t, \quad (7)$$

where $c = \frac{\eta \alpha^2}{r^2}$ is a positive constant integrating the learning rate and LoRA scaling effects.

Remark. Proposition 3.1 reveals that frozen \mathbf{A}_t updates are inherently subspace constrained: all changes to \mathbf{W} are confined to $\text{span}(\mathbf{A}_t)$, as $\mathbf{A}_t \mathbf{A}_t^\top$ acts as an orthogonal projection operator on this subspace. Furthermore, $\text{span}(\mathbf{A}_t)$ requires satisfying the following two properties in continual learning: (i) Orthogonal to knowledge subspaces: $\text{span}(\mathbf{A}_t)$ need to be orthogonal to subspaces encoding pre-trained knowledge and previously learned tasks, ensuring updates to \mathbf{W} do not interfere with existing knowledge, preventing both forward and backward forgetting. (ii) Adaptation to the current task: $\text{span}(\mathbf{A}_t)$ needs to capture the dominant directions of \mathbf{G}_t , approximating the gradient of full-parameter fine-tuning to maintain plasticity.

Validation of KeepLoRA \mathbf{A}_t Initialization. The preceding proposition outlines the required properties of $\text{span}(\mathbf{A}_t)$. The key question is whether the KeepLoRA initialization of \mathbf{A}_t meets the two properties. We validate it by connecting the initialization to a constrained optimization problem.

Proposition 3.2. *KeepLoRA initialization of \mathbf{A}_t through Eq. 5 and Eq. 6 is the solution to the following constrained optimization problem:*

$$\begin{aligned} & \min_{\mathbf{A}_t^\top \mathbf{A}_t = \mathbf{I}} \|\mathbf{G}_t - \mathbf{A}_t \mathbf{A}_t^\top \mathbf{G}_t\|_F^2, \\ & \text{s.t. } \mathbf{W}_p^\top \mathbf{A}_t = \mathbf{M}_{t-1}^\top \mathbf{A}_t = \mathbf{0}, \end{aligned} \quad (8)$$

where \mathbf{G}_t is the current task gradient w.r.t. the base model \mathbf{W} , \mathbf{W}_p is the principal subspace of pre-trained parameters, and \mathbf{M}_{t-1} is the dominant feature directions from previous tasks.

Remark. Proposition 3.2 directly connects KeepLoRA’s initialization technique to the two properties of Proposition 3.1, verifying its optimality: (i) Satisfying orthogonality (via constraints): The equality constraints $\mathbf{W}_p^\top \mathbf{A}_t = \mathbf{0}$ and $\mathbf{M}_{t-1}^\top \mathbf{A}_t = \mathbf{0}$ explicitly enforce $\text{span}(\mathbf{A}_t) \perp \text{span}(\mathbf{W}_p)$ and $\text{span}(\mathbf{A}_t) \perp \text{span}(\mathbf{M}_{t-1})$. It guarantees that $\text{span}(\mathbf{A}_t)$ is orthogonal to both the principal subspace of the model parameters and the dominant feature directions to preserve stability. (ii) Optimal adaptation (via objective): The objective function minimizes the Frobenius norm of $\mathbf{G}_t - \mathbf{A}_t \mathbf{A}_t^\top \mathbf{G}_t$, the residual component of \mathbf{G}_t that lies outside $\text{span}(\mathbf{A}_t)$. By the Pythagorean theorem for the Frobenius

Table 2: Comparison of different methods on MTIL for each **classification** task in terms of *Transfer*, *Average*, and *Last* scores (%). The best results are in **bold**.

| Method | | Arch. | Kept | w/o Extra Data | Aircraft | Caltech101 | CIFAR100 | DTD | EuroSAT | Flowers | Food | MNIST | OxfordPet | Cars | Sun397 | Avg. |
|---------------------------------|--|-------|------|----------------|-------------|-------------|-------------|-------------|-------------|-------------|-------------|-------------|-------------|-------------|-------------|------|
| Zero-shot | | ✓ | ✓ | 24.8 | 88.4 | 68.2 | 44.6 | 54.9 | 71.0 | 88.5 | 59.4 | 89.0 | 64.7 | 65.4 | | |
| Transfer | | | | | | | | | | | | | | | | |
| LwF (Li & Hoiem, 2017) | | ✓ | ✗ | — | 74.5 | 56.9 | 39.1 | 51.1 | 52.6 | 72.8 | 60.6 | 75.1 | 30.3 | 55.9 | 56.9 | |
| iCaRL (Rebuffi et al., 2017) | | ✓ | ✗ | — | 56.6 | 44.6 | 32.7 | 39.3 | 46.6 | 68.0 | 46.0 | 77.4 | 31.9 | 60.5 | 50.4 | |
| LwF-VR (Ding et al., 2022) | | ✓ | ✗ | — | 77.1 | 61.0 | 40.5 | 45.3 | 54.4 | 74.6 | 47.9 | 76.7 | 36.3 | 58.6 | 57.2 | |
| WiSE-FT (Wortsman et al., 2022) | | ✓ | ✗ | — | 73.5 | 55.6 | 35.6 | 41.5 | 47.0 | 68.3 | 53.9 | 69.3 | 26.8 | 51.9 | 52.3 | |
| ZSCL (Zheng et al., 2023) | | ✓ | ✗ | — | 86.0 | 67.4 | 45.4 | 50.4 | 69.1 | 87.6 | 61.8 | 86.8 | 60.1 | 66.8 | 68.1 | |
| O-LoRA (Wang et al., 2023a) | | ✓ | ✓ | — | 80.8 | 68.0 | 44.5 | 49.8 | 67.5 | 86.7 | 59.3 | 88.7 | 56.1 | 63.6 | 66.5 | |
| InfLoRA (Liang & Li, 2024) | | ✓ | ✓ | — | 84.3 | 67.4 | 44.3 | 50.6 | 68.2 | 87.1 | 62.7 | 88.7 | 57.8 | 62.8 | 67.4 | |
| SD-LoRA (Wu et al., 2025b) | | ✓ | ✓ | — | 82.3 | 67.5 | 44.4 | 51.0 | 67.9 | 87.2 | 61.1 | 88.4 | 58.2 | 63.4 | 67.1 | |
| KeepLoRA | | ✓ | ✓ | — | 84.6 | 68.7 | 45.9 | 54.3 | 70.1 | 87.7 | 64.8 | 90.3 | 59.5 | 64.1 | 69.0 | |
| L2P (Wang et al., 2022c) | | ✗ | ✓ | — | 65.6 | 50.9 | 30.4 | 41.4 | 49.3 | 71.8 | 36.3 | 77.5 | 55.3 | 53.4 | 53.2 | |
| DualPrompt (Wang et al., 2022b) | | ✗ | ✓ | — | 56.7 | 51.4 | 28.7 | 33.7 | 45.6 | 70.9 | 59.5 | 77.7 | 49.5 | 50.4 | 52.4 | |
| S-Prompts (Wang et al., 2022a) | | ✗ | ✓ | — | 67.3 | 49.4 | 26.7 | 39.7 | 47.1 | 70.2 | 34.3 | 78.9 | 56.7 | 52.2 | 52.2 | |
| DIKI (Tang et al., 2024) | | ✗ | ✓ | — | 92.9 | 69.1 | 43.2 | 43.9 | 65.4 | 85.3 | 56.0 | 88.4 | 64.0 | 65.6 | 67.4 | |
| MoE-Adapters (Yu et al., 2024) | | ✗ | ✗ | — | 87.9 | 68.2 | 44.4 | 49.9 | 70.7 | 88.7 | 59.7 | 89.1 | 64.5 | 65.5 | 68.9 | |
| IAP (Fu et al., 2025) | | ✗ | ✓ | — | 93.0 | 68.7 | 44.0 | 47.0 | 70.4 | 85.9 | 63.5 | 89.7 | 66.2 | 63.3 | 69.2 | |
| KeepLoRA+ | | ✗ | ✓ | — | 85.9 | 69.9 | 44.6 | 53.7 | 70.9 | 88.9 | 65.4 | 90.8 | 63.0 | 66.1 | 69.9 | |
| Average | | | | | | | | | | | | | | | | |
| LwF (Li & Hoiem, 2017) | | ✓ | ✗ | 36.3 | 86.9 | 72.0 | 59.0 | 73.7 | 60.0 | 73.6 | 74.8 | 80.0 | 37.3 | 58.1 | 64.7 | |
| iCaRL (Rebuffi et al., 2017) | | ✓ | ✗ | 35.5 | 89.2 | 72.2 | 60.6 | 68.8 | 70.0 | 78.2 | 62.3 | 81.8 | 41.2 | 62.5 | 65.7 | |
| LwF-VR (Ding et al., 2022) | | ✓ | ✗ | 29.6 | 87.7 | 74.4 | 59.5 | 72.4 | 63.6 | 77.0 | 66.7 | 81.2 | 43.7 | 60.7 | 65.1 | |
| WiSE-FT (Wortsman et al., 2022) | | ✓ | ✗ | 26.7 | 86.5 | 64.3 | 57.1 | 65.7 | 58.7 | 71.1 | 70.5 | 75.8 | 36.9 | 54.6 | 60.7 | |
| ZSCL (Zheng et al., 2023) | | ✓ | ✗ | 45.1 | 92.0 | 80.1 | 64.3 | 79.5 | 81.6 | 89.6 | 75.2 | 88.9 | 64.7 | 68.0 | 75.4 | |
| O-LoRA (Wang et al., 2023a) | | ✓ | ✓ | 39.8 | 93.2 | 78.3 | 61.7 | 78.9 | 76.3 | 88.5 | 73.9 | 90.1 | 60.2 | 65.2 | 73.3 | |
| InfLoRA (Liang & Li, 2024) | | ✓ | ✓ | 53.6 | 95.6 | 82.8 | 65.0 | 80.9 | 79.6 | 89.1 | 76.1 | 90.2 | 62.3 | 64.5 | 76.3 | |
| SD-LoRA (Wu et al., 2025b) | | ✓ | ✓ | 36.7 | 92.2 | 80.2 | 55.9 | 77.5 | 73.2 | 89.2 | 74.9 | 89.8 | 62.5 | 65.0 | 72.5 | |
| KeepLoRA | | ✓ | ✓ | 55.6 | 95.7 | 83.2 | 65.6 | 82.2 | 82.0 | 89.5 | 77.4 | 91.5 | 63.9 | 65.8 | 77.5 | |
| L2P (Wang et al., 2022c) | | ✗ | ✓ | 38.0 | 85.2 | 78.2 | 61.3 | 72.9 | 74.9 | 79.7 | 59.1 | 82.0 | 59.7 | 55.4 | 67.9 | |
| DualPrompt (Wang et al., 2022b) | | ✗ | ✓ | 37.8 | 84.3 | 78.6 | 60.1 | 71.1 | 73.2 | 79.1 | 73.9 | 82.3 | 55.1 | 52.8 | 68.0 | |
| S-Prompts (Wang et al., 2022a) | | ✗ | ✓ | 37.5 | 92.5 | 77.5 | 58.2 | 76.4 | 74.1 | 78.8 | 57.9 | 83.0 | 60.8 | 54.4 | 68.3 | |
| DIKI (Tang et al., 2024) | | ✗ | ✓ | 45.4 | 95.7 | 83.0 | 65.0 | 78.2 | 82.5 | 87.1 | 71.7 | 90.0 | 67.2 | 66.6 | 75.7 | |
| MoE-Adapters (Yu et al., 2024) | | ✗ | ✗ | 50.2 | 91.9 | 83.1 | 69.4 | 78.9 | 84.0 | 89.1 | 73.7 | 89.3 | 67.7 | 66.9 | 76.7 | |
| IAP (Fu et al., 2025) | | ✗ | ✓ | 45.9 | 95.8 | 83.3 | 66.5 | 79.5 | 84.8 | 87.5 | 76.6 | 91.0 | 69.2 | 64.5 | 76.8 | |
| KeepLoRA+ | | ✗ | ✓ | 58.4 | 96.5 | 84.4 | 67.8 | 82.1 | 84.5 | 90.7 | 77.8 | 91.9 | 67.5 | 67.6 | 79.0 | |
| Last | | | | | | | | | | | | | | | | |
| LwF (Li & Hoiem, 2017) | | ✓ | ✗ | 26.3 | 87.5 | 71.9 | 66.6 | 79.9 | 66.9 | 83.8 | 99.6 | 92.1 | 66.1 | 80.4 | 74.6 | |
| iCaRL (Rebuffi et al., 2017) | | ✓ | ✗ | 35.8 | 93.0 | 77.0 | 70.2 | 83.3 | 88.5 | 90.4 | 86.7 | 93.2 | 81.2 | 81.9 | 80.1 | |
| LwF-VR (Ding et al., 2022) | | ✓ | ✗ | 20.5 | 89.8 | 72.3 | 67.6 | 85.5 | 73.8 | 85.7 | 99.6 | 93.1 | 73.3 | 80.9 | 76.6 | |
| WiSE-FT (Wortsman et al., 2022) | | ✓ | ✗ | 27.2 | 90.8 | 68.0 | 68.9 | 86.9 | 74.0 | 87.6 | 99.6 | 92.6 | 77.8 | 81.3 | 77.7 | |
| ZSCL (Zheng et al., 2023) | | ✓ | ✗ | 40.6 | 92.2 | 81.3 | 70.5 | 94.8 | 90.5 | 91.9 | 98.7 | 93.9 | 85.3 | 80.2 | 83.6 | |
| O-LoRA (Wang et al., 2023a) | | ✓ | ✓ | 31.4 | 91.8 | 75.7 | 61.1 | 89.0 | 76.0 | 88.9 | 99.1 | 92.3 | 74.8 | 81.3 | 78.3 | |
| InfLoRA (Liang & Li, 2024) | | ✓ | ✓ | 51.1 | 96.5 | 85.1 | 70.7 | 98.1 | 87.7 | 91.3 | 99.4 | 94.2 | 82.0 | 81.4 | 85.2 | |
| SD-LoRA (Wu et al., 2025b) | | ✓ | ✓ | 31.1 | 92.3 | 79.8 | 57.4 | 88.7 | 76.1 | 90.6 | 99.0 | 92.9 | 81.3 | 81.6 | 79.2 | |
| KeepLoRA | | ✓ | ✓ | 53.2 | 96.8 | 85.7 | 71.4 | 98.1 | 90.8 | 91.4 | 99.6 | 94.5 | 83.1 | 82.0 | 86.1 | |
| L2P (Wang et al., 2022c) | | ✗ | ✓ | 38.0 | 87.1 | 84.2 | 72.9 | 86.0 | 96.1 | 89.2 | 99.0 | 94.1 | 79.6 | 76.0 | 82.0 | |
| DualPrompt (Wang et al., 2022b) | | ✗ | ✓ | 37.8 | 87.1 | 84.6 | 71.8 | 89.2 | 96.3 | 89.1 | 99.1 | 94.5 | 79.9 | 76.5 | 82.3 | |
| S-Prompts (Wang et al., 2022a) | | ✗ | ✓ | 37.5 | 95.1 | 83.7 | 70.2 | 97.5 | 96.5 | 89.0 | 99.1 | 94.0 | 79.5 | 75.8 | 83.4 | |
| DIKI (Tang et al., 2024) | | ✗ | ✓ | 45.4 | 95.9 | 86.0 | 73.0 | 97.8 | 96.8 | 89.3 | 99.3 | 94.4 | 81.8 | 76.4 | 85.1 | |
| MoE-Adapters (Yu et al., 2024) | | ✗ | ✗ | 49.8 | 92.2 | 86.1 | 78.1 | 95.7 | 94.3 | 89.5 | 98.1 | 89.9 | 81.6 | 80.0 | 85.0 | |
| IAP (Fu et al., 2025) | | ✗ | ✓ | 46.8 | 96.1 | 86.7 | 75.2 | 98.1 | 97.0 | 89.6 | 99.4 | 94.7 | 82.8 | 76.7 | 85.7 | |
| KeepLoRA+ | | ✗ | ✓ | 57.3 | 97.6 | 87.2 | 76.5 | 98.4 | 95.7 | 92.6 | 99.5 | 94.7 | 87.2 | 83.2 | 88.2 | |

norms ($\|G_t\|_F^2 = \|\mathbf{A}_t \mathbf{A}_t^\top G_t\|_F^2 + \|G_t - \mathbf{A}_t \mathbf{A}_t^\top G_t\|_F^2$), minimizing this residual is equivalent to maximizing the norm of the projected gradient $\mathbf{A}_t \mathbf{A}_t^\top G_t$. It ensures $\text{span}(\mathbf{A}_t)$ captures the dominant gradient directions for the current task, preserving plasticity.

In summary, Propositions 3.1 and 3.2 form a complete theoretical loop: Proposition 3.1 defines the necessary properties of $\text{span}(\mathbf{A}_t)$ for stable-plastic continual learning. Proposition 3.2 further proves that the initialization technique of \mathbf{A}_t in KeepLoRA is aligned with these properties, which ensures that $\text{span}(\mathbf{A}_t)$ is orthogonal to the principal subspace of the model parameters \mathbf{W}_p and dominant feature directions of each learned task M_{t-1} to maintain stability, while being adaptive to the current task gradient to improve plasticity.

4 EXPERIMENTS

We conduct experiments on various benchmarks to validate the effectiveness of KeepLoRA in balancing three core objectives of continual learning: forward stability, backward stability, and plasticity. (i) To quantify forward forgetting, we calculate the average accuracy on tasks $t+1, \dots, n$ after training on task t , which is defined as the *Transfer* metric, presented in Tab. 2, 3 and 4. Fig. 2 further analyzes how KeepLoRA maintains the transferability. (ii) The *Last* metric, shown in Tab. 2, 3 and 4, assesses model performance after continual training has completed, capturing both plasticity and backward stability. (iii) To further analyze plasticity, Fig. 3 compares our method with an unconstrained LoRA, demonstrating that KeepLoRA preserves stability with minimal sacrifice to its adaptive capability. The *Average* metric represents the mean accuracy across all learned tasks, offering a holistic measure of the balance between stability and plasticity.

Table 3: Comparison of different continual learning methods on MLLM-DCL benchmark for **VQA** tasks in terms of *Transfer*, *Average*, and *Last* scores (%). The best results are in **bold**.

| Method | Sensing | Medical | Driving | Science | Finance | Avg. |
|-----------------------------|--------------|--------------|--------------|--------------|--------------|--------------|
| Zero-shot | 32.29 | 28.28 | 15.59 | 35.55 | 62.56 | |
| Transfer | | | | | | |
| LoRA-FT (Hu et al., 2022) | – | 28.10 | 17.44 | 34.03 | 50.19 | 32.44 |
| O-LoRA (Wang et al., 2023a) | – | 28.37 | 18.37 | 33.72 | 52.53 | 33.25 |
| CL-MoE (Huai et al., 2025) | – | 28.25 | 19.38 | 34.08 | 48.56 | 32.57 |
| SEFE (Chen et al., 2025) | – | 28.10 | 19.63 | 33.85 | 52.36 | 33.49 |
| KeepLoRA | – | 28.49 | 16.63 | 34.13 | 55.61 | 33.71 |
| Average | | | | | | |
| LoRA-FT (Hu et al., 2022) | 73.34 | 44.94 | 31.38 | 38.79 | 57.84 | 49.26 |
| O-LoRA (Wang et al., 2023a) | 75.04 | 45.71 | 32.62 | 38.54 | 59.64 | 50.31 |
| CL-MoE (Huai et al., 2025) | 74.19 | 45.60 | 32.08 | 38.88 | 56.68 | 49.49 |
| SEFE (Chen et al., 2025) | 77.71 | 47.69 | 35.35 | 38.99 | 59.57 | 51.86 |
| KeepLoRA | 79.55 | 50.80 | 37.53 | 40.70 | 62.35 | 54.19 |
| Last | | | | | | |
| LoRA-FT (Hu et al., 2022) | 69.34 | 44.30 | 29.10 | 41.44 | 88.43 | 54.52 |
| O-LoRA (Wang et al., 2023a) | 72.30 | 46.89 | 31.59 | 41.50 | 88.06 | 56.07 |
| CL-MoE (Huai et al., 2025) | 71.83 | 47.36 | 29.49 | 41.48 | 89.16 | 55.86 |
| SEFE (Chen et al., 2025) | 77.05 | 50.86 | 40.27 | 42.98 | 88.40 | 59.91 |
| KeepLoRA | 78.76 | 54.34 | 50.19 | 49.48 | 89.30 | 64.41 |

4.1 MAIN RESULTS

We evaluate our method on the dual-encoder model CLIP (Radford et al., 2021) and encoder-decoder model LLaVA (Liu et al., 2023). For CLIP, the experiments are conducted on the MTIL (Zheng et al., 2023) benchmark, presenting results for alphabetical (Tab. 2) and random (Tab. 6) task orders in two settings, with and without architecture extension. KeepLoRA+ is a structure extension variant with a prototype vector for a class name to help classification, which is detailed in Appendix B.3. For LLaVA, the experiments (Tab. 3 and 4) are conducted on MLLM-DCL (Guo et al., 2025b) and UCIT (Guo et al., 2025b) benchmarks, including various instruction formats such as image

Table 4: Comparison of different continual learning methods on UCIT benchmark for **VQA** tasks in terms of *Transfer*, *Average*, and *Last* scores (%). The best results are in **bold**.

| Method | ImgNet-R | ArxivQA | VizWiz | IconQA | CLEVR | Flickr30k | Avg. |
|-----------------------------|--------------|--------------|--------------|--------------|--------------|--------------|--------------|
| Zero-shot | 16.27 | 53.73 | 38.39 | 19.20 | 20.63 | 41.88 | |
| Transfer | | | | | | | |
| LoRA-FT (Hu et al., 2022) | — | 52.63 | 18.30 | 6.02 | 16.97 | 40.29 | 26.84 |
| O-LoRA (Wang et al., 2023a) | — | <u>52.87</u> | <u>19.57</u> | 4.42 | 16.85 | 41.04 | 26.95 |
| CL-MoE (Huai et al., 2025) | — | 52.00 | 19.32 | 7.37 | <u>17.81</u> | <u>41.28</u> | <u>27.56</u> |
| SEFE (Chen et al., 2025) | — | 53.33 | 18.68 | <u>7.48</u> | 17.03 | 40.90 | 27.48 |
| KeepLoRA | — | 52.83 | 20.39 | 9.18 | 18.12 | 41.50 | 28.40 |
| Average | | | | | | | |
| LoRA-FT (Hu et al., 2022) | 75.98 | 77.78 | 41.56 | 38.83 | 34.56 | 43.25 | 51.99 |
| O-LoRA (Wang et al., 2023a) | 82.43 | <u>80.06</u> | 41.73 | 35.87 | 33.94 | 43.74 | 52.96 |
| CL-MoE (Huai et al., 2025) | 80.16 | <u>77.10</u> | 40.43 | 30.33 | 33.10 | <u>43.95</u> | 50.85 |
| SEFE (Chen et al., 2025) | 85.49 | 78.55 | 42.92 | 40.33 | <u>34.80</u> | <u>43.64</u> | <u>54.29</u> |
| KeepLoRA | 86.50 | 83.63 | 42.66 | 40.08 | 35.24 | 44.11 | 55.37 |
| Last | | | | | | | |
| LoRA-FT (Hu et al., 2022) | 58.60 | 76.73 | 45.72 | 67.43 | 61.57 | 58.03 | 61.35 |
| O-LoRA (Wang et al., 2023a) | 74.17 | <u>80.93</u> | 45.30 | 62.87 | 63.83 | 57.24 | 64.06 |
| CL-MoE (Huai et al., 2025) | 67.17 | <u>75.77</u> | 44.38 | 52.63 | 54.40 | 57.28 | 58.61 |
| SEFE (Chen et al., 2025) | 80.23 | 79.13 | 47.11 | 69.40 | 65.70 | 57.33 | 66.48 |
| KeepLoRA | 82.43 | 86.70 | <u>46.54</u> | <u>67.80</u> | 66.40 | 57.18 | 67.84 |

captioning, visual question-answer, and multiple-choice questions. Detailed information on experiment settings and benchmarks is presented in Appendices B.4 and B.1, separately. KeepLoRA and KeepLoRA+ achieve state-of-the-art performance on the *Transfer*, *Average*, and *Last* metrics in each of these settings. This demonstrates that our approach consistently addresses the challenges of forward stability, backward stability, and plasticity in continual learning.

4.2 ANALYSIS OF MODEL STABILITY

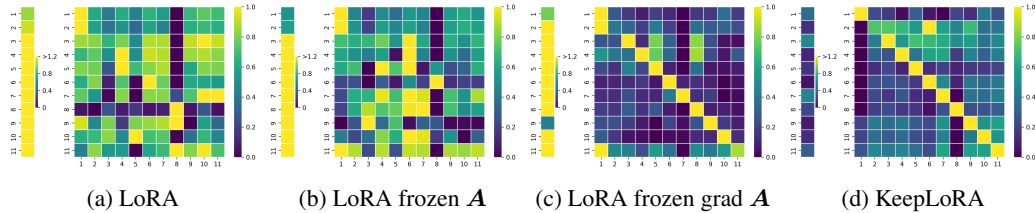


Figure 2: Visualization of the average L2 norm of the output magnitude from the learned LoRA across multiple tasks. Each heatmap cell at row i and column j displays the normalized average L2 norm of the LoRA’s output when the model, trained up to task i , is tested on task j ’s data. The vertical bar to the left of each heatmap indicates the mean output norm across all test tasks after each training stage, with darker colors signifying a lower norm and thus a reduced impact on the stability.

We analyze stability by visualizing the interference of the LoRA module between multiple tasks in Fig. 2. In these heatmaps, the off-diagonal cells represent inter-task interference, while the vertical bar on the left indicates the overall impact on the backbone. The standard LoRA (Fig. 2a) and LoRA with a frozen matrix A (Fig. 2b) both exhibit significant interference. The bright patterns in their heatmaps and vertical bars show that training on a current task heavily interferes with the representations of other tasks, leading to poor stability. Although gradient-informed initialization (Fig. 2c) reduces off-diagonal interference, the overall impact on the backbone remains high, as shown by its bright vertical bar. In contrast, KeepLoRA (Fig. 2d) shows a desirable pattern: a bright diagonal with dark off-diagonal cells. This indicates that the updates of the model are focused on the current task, causing minimal interference with others. The dark vertical bar further confirms that

the overall impact on the backbone is consistently low. By minimizing interference with previously learned tasks, KeepLoRA ensures backward stability. Furthermore, its minimal interference with unseen tasks, as indicated by the low norm, is critical for preserving forward stability.

4.3 ANALYSIS OF MODEL PLASTICITY

Plasticity assesses the ability to effectively acquire new knowledge following a sequence of continual learning tasks. We evaluate two performance metrics for each task: (i) the accuracy achieved by training on the task in isolation, serving as an upper bound, and (ii) the accuracy measured immediately after the task is learned within the continual sequence. Our analysis in Fig. 3 compares KeepLoRA with a standard LoRA baseline. In the isolation-task setting, KeepLoRA performs comparably to LoRA, as gradient-informed initialization of the frozen down-projection matrix \mathbf{A} effectively captures the essential learning direction, maintaining high learning capacity. Furthermore, when switching to the continual learning scenario, KeepLoRA exhibits a consistently smaller performance drop on new tasks compared to LoRA. This suggests that, by confining updates to the residual subspace and avoiding interference with previously learned knowledge, our method enhances the model’s plasticity for subsequent tasks.

4.4 ABLATION STUDY

To analyze the contribution of each component, we conduct an ablation study starting from a standard LoRA baseline. As shown in Tab. 5, our modifications progressively improve performance. Freezing the down-projection matrix \mathbf{A} even with random initialization, enhances stability in the continual learning setting by mitigating destructive interference with the backbone weights. Subsequently, employing a (i) gradient-informed initialization further improves plasticity, leading to a 5.9% increase on the *Last* metric and indicating more effective adaptation. After constraining the updates to be orthogonal to (ii) the principal subspace \mathbf{W}_p and (iii) the dominant feature directions \mathbf{M} , gains of 4.0% on *Transfer*, 7.3% on *Average*, and 10.7% on *Last*, demonstrating the critical role of subspace projection in balancing stability and plasticity.

Table 5: Ablation Study of KeepLoRA on MTIL.

| Training Strategy | Transfer | Δ | Average | Δ | Last | Δ |
|--|----------|----------|---------|----------|------|----------|
| LoRA (rank 8, # param. 0.98 M) | 58.3 | 0.0 | 61.5 | 0.0 | 59.4 | 0.0 |
| LoRA frozen \mathbf{A} (rank 16, # param. 0.98 M) | 63.9 | +5.6 | 68.2 | +6.7 | 69.5 | +10.1 |
| (i) Replace Eq. 5 by $\hat{\mathbf{G}}_t = \mathbf{G}_t$ | 65.0 | +6.7 | 70.2 | +8.7 | 75.4 | +16.0 |
| (ii) Replace Eq. 5 by $\hat{\mathbf{G}}_t = \mathbf{G}_t - \mathbf{W}_p \mathbf{W}_p^\top \mathbf{G}_t$ | 65.9 | +7.6 | 71.5 | +10.0 | 76.5 | +17.1 |
| (iii) Replace Eq. 5 by $\hat{\mathbf{G}}_t = \mathbf{G}_t - \mathbf{M}_{t-1} \mathbf{M}_{t-1}^\top \mathbf{G}_t$ | 68.1 | +9.8 | 77.2 | +15.7 | 86.1 | +26.7 |
| KeepLoRA (Eq. 5) | 69.0 | +10.7 | 77.5 | +16.0 | 86.1 | +26.7 |

5 CONCLUSION

This work is motivated by the observation that the principal subspace of parameters encodes general knowledge and the residual subspace captures domain-specific adaptations. Building on this, we proposed KeepLoRA, a parameter-efficient fine-tuning method that can effectively achieve a balance among the competing objectives of plasticity, backward stability, and forward stability. Our

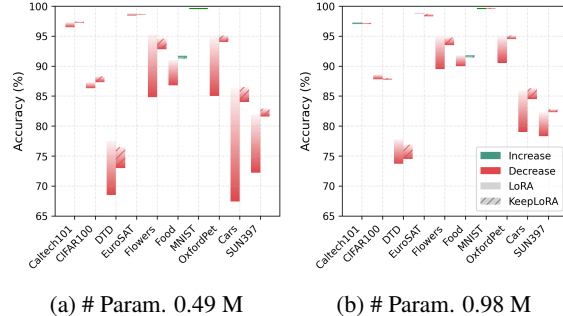


Figure 3: Comparison of plasticity between KeepLoRA and the LoRA baseline under the same learnable parameter budgets: Fig. 3a 0.49 million parameters and Fig. 3b 0.98 million parameters. Each bar represents the performance drop for a task, measured as the difference between accuracy from isolated training and accuracy after sequential learning and immediate testing.

This suggests that, by confining updates to the residual subspace and avoiding interference with previously learned knowledge, our method enhances the model’s plasticity for subsequent tasks.

theoretical analysis confirms that constraining parameter updates to the residual subspace is an optimal strategy, maximizing plasticity for the current task while maintaining orthogonality to subspaces encoding general and previously learned knowledge. Experiments show that KeepLoRA learns new tasks with minimal interference with the model’s backbone parameters. Its learning capacity within the residual subspace is comparable to unconstrained LoRA on isolated tasks, yet it suffers a significantly smaller performance drop in the continual learning setting. As a simple and effective method, KeepLoRA provides a principled approach for continual learning that is applicable to larger models and more diverse tasks.

ETHICS STATEMENT

All authors have read and adhered to the ICLR Code of Ethics. This paper presents an algorithmic contribution, KeepLoRA, aimed at advancing the field of continual learning. Our empirical validation is conducted exclusively on publicly available and widely used academic benchmarks, such as CIFAR100 and Caltech101, which do not contain personally identifiable or sensitive information. While we acknowledge that advancements in machine learning have broad societal consequences, our work does not introduce foreseeable negative applications or exacerbate biases beyond those potentially present in the general pre-trained models.

REPRODUCIBILITY STATEMENT

To ensure full reproducibility, we provide the source code for our method, KeepLoRA, in the supplementary material. Our method is detailed in Sec. 3, with the core framework summarized in Algorithm 1. We specify all hyperparameters used for our method and the baselines, including learning rates, batch size, and the preservation ratios ϵ_w and ϵ_f in Appendix B.

REFERENCES

Josh Achiam, Steven Adler, Sandhini Agarwal, Lama Ahmad, Ilge Akkaya, Florencia Leoni Aleman, Diogo Almeida, Janko Altenschmidt, Sam Altman, Shyamal Anadkat, et al. Gpt-4 technical report. *arXiv preprint arXiv:2303.08774*, 2023.

Lukas Bossard, Matthieu Guillaumin, and Luc Van Gool. Food-101–mining discriminative components with random forests. In *European conference of computer vision (ECCV)*, 2014.

Weilin Cai, Juyong Jiang, Fan Wang, Jing Tang, Sunghun Kim, and Jiayi Huang. A survey on mixture of experts in large language models. *IEEE Transactions on Knowledge and Data Engineering*, 2025.

Shuaichen Chang, David Palzer, Jialin Li, Eric Fosler-Lussier, and Ningchuan Xiao. Mapqa: A dataset for question answering on choropleth maps. In *arXiv preprint arXiv:2211.08545*, 2022.

Jinpeng Chen, Runmin Cong, Yuzhi Zhao, Hongzheng Yang, Guangneng Hu, Horace Ho Shing Ip, and Sam Kwong. Sefe: Superficial and essential forgetting eliminator for multimodal continual instruction. In *Proceedings of the IEEE/CVF Conference on Computer Vision and Pattern Recognition (CVPR)*, 2025.

Quan Cheng, Yuanyu Wan, Lingyu Wu, Chenping Hou, and Lijun Zhang. Continuous subspace optimization for continual learning. *arXiv preprint arXiv:2505.11816*, 2025.

Mircea Cimpoi, Subhransu Maji, Iasonas Kokkinos, Sammy Mohamed, and Andrea Vedaldi. Describing textures in the wild. In *Proceedings of the IEEE conference on computer vision and pattern recognition (CVPR)*, 2014.

Gheorghe Comanici, Eric Bieber, Mike Schaeckermann, Ice Pasupat, Noveen Sachdeva, Inderjit Dhillon, Marcel Blstein, Ori Ram, Dan Zhang, Evan Rosen, et al. Gemini 2.5: Pushing the frontier with advanced reasoning, multimodality, long context, and next generation agentic capabilities. *arXiv preprint arXiv:2507.06261*, 2025.

Gregoire Deletang, Anian Ruoss, Paul-Ambroise Duquenne, Elliot Catt, Tim Genewein, Christopher Mattern, Jordi Grau-Moya, Li Kevin Wenliang, Matthew Aitchison, Laurent Orseau, et al. Language modeling is compression. In *The Twelfth International Conference on Learning Representations*, 2024.

Jia Deng, Wei Dong, Richard Socher, Li-Jia Li, Kai Li, and Li Fei-Fei. Imagenet: A large-scale hierarchical image database. In *2009 IEEE conference on computer vision and pattern recognition*, pp. 248–255. Ieee, 2009.

Li Deng. The mnist database of handwritten digit images for machine learning research [best of the web]. *IEEE signal processing magazine*, 2012.

Yuxuan Ding, Lingqiao Liu, Chunna Tian, Jingyuan Yang, and Haoxuan Ding. Don’t stop learning: Towards continual learning for the clip model. *arXiv preprint arXiv:2207.09248*, 2022.

Alexey Dosovitskiy, Lucas Beyer, Alexander Kolesnikov, Dirk Weissenborn, Xiaohua Zhai, Thomas Unterthiner, Mostafa Dehghani, Matthias Minderer, Georg Heigold, Sylvain Gelly, Jakob Uszkoreit, and Neil Houlsby. An image is worth 16x16 words: Transformers for image recognition at scale. In *International Conference on Learning Representations (ICLR)*, 2021.

Shihan Dou, Enyu Zhou, Yan Liu, Songyang Gao, Wei Shen, Limao Xiong, Yuhao Zhou, Xiao Wang, Zhiheng Xi, Xiaoran Fan, et al. Loramoe: Alleviating world knowledge forgetting in large language models via moe-style plugin. In *Proceedings of the 62nd Annual Meeting of the Association for Computational Linguistics (Volume 1: Long Papers)*, pp. 1932–1945, 2024.

Carl Eckart and Gale Young. The approximation of one matrix by another of lower rank. *Psychometrika*, 1936.

Li Fei-Fei, Rob Fergus, and Pietro Perona. Learning generative visual models from few training examples: An incremental bayesian approach tested on 101 object categories. In *Conference on computer vision and pattern recognition workshop*, 2004.

Giorgio Franceschelli, Claudia Cevenini, and Mirco Musolesi. Training foundation models as data compression: On information, model weights and copyright law. *arXiv preprint arXiv:2407.13493*, 2024.

Hao Fu, Hanbin Zhao, Jiahua Dong, Chao Zhang, and Hui Qian. Iap: Improving continual learning of vision-language models via instance-aware prompting. *arXiv preprint arXiv:2503.20612*, 2025.

H. Guo, F. Zeng, Z. Xiang, et al. Hide-llava: Hierarchical decoupling for continual instruction tuning of multimodal large language model. In *arXiv preprint arXiv:2503.12941*, 2025a.

Haiyang Guo, Fei Zhu, Hongbo Zhao, Fanhu Zeng, Wenzhuo Liu, Shijie Ma, Da-Han Wang, and Xu-Yao Zhang. Mcitlib: Multimodal continual instruction tuning library and benchmark. *arXiv preprint arXiv:2508.07307*, 2025b.

Ziyu Guo, Ray Zhang, Hao Chen, Jialin Gao, Dongzhi Jiang, Jiaze Wang, and Pheng-Ann Heng. Sciverse: Unveiling the knowledge comprehension and visual reasoning of lmms on multi-modal scientific problems. In *Findings of the Association for Computational Linguistics: ACL 2025*, pp. 19683–19704, 2025c.

Danna Gurari, Qing Li, Abigale J Stangl, Anhong Guo, Chi Lin, Kristen Grauman, Jiebo Luo, and Jeffrey P Bigham. Vizwiz grand challenge: Answering visual questions from blind people. In *Proceedings of the IEEE Conference on Computer Vision and Pattern Recognition (CVPR)*, pp. 3608–3617, 2018.

Xuehai He, Yichen Zhang, Luntian Mou, Eric Xing, and Pengtao Xie. Pathvqa: 30000+ questions for medical visual question answering. In *arXiv preprint arXiv:2003.10286*, 2020.

Patrick Helber, Benjamin Bischke, Andreas Dengel, and Damian Borth. Eurosat: A novel dataset and deep learning benchmark for land use and land cover classification. *IEEE Journal of selected topics in applied earth observations and remote sensing*, 2019.

Dan Hendrycks, Steven Basart, Norman Mu, et al. The many faces of robustness: A critical analysis of out-of-distribution generalization. In *Proceedings of the IEEE/CVF International Conference on Computer Vision (ICCV)*, pp. 8340–8349, 2021.

Edward J Hu, Yelong Shen, Phillip Wallis, Zeyuan Allen-Zhu, Yuanzhi Li, Shean Wang, Lu Wang, Weizhu Chen, et al. Lora: Low-rank adaptation of large language models. *ICLR*, 1(2):3, 2022.

Tianyu Huai, Jie Zhou, Xingjiao Wu, Qin Chen, Qingchun Bai, Ze Zhou, and Liang He. Cl-moe: Enhancing multimodal large language model with dual momentum mixture-of-experts for continual visual question answering. In *Proceedings of the IEEE/CVF Conference on Computer Vision and Pattern Recognition*, pp. 19608–19617, 2025.

Aniruddha Kembhavi, Mike Salvato, Eric Kolve, Minjoon Seo, Hannaneh Hajishirzi, and Ali Farhadi. A diagram is worth a dozen images. In *European Conference on Computer Vision (ECCV)*, pp. 235–251. Springer, 2016.

Aniruddha Kembhavi, Minjoon Seo, Dustin Schwenk, Jonghyun Choi, Ali Farhadi, and Hannaneh Hajishirzi. Are you smarter than a sixth grader? textbook question answering for multimodal machine comprehension. In *Proceedings of the IEEE Conference on Computer Vision and Pattern Recognition (CVPR)*, pp. 4999–5007, 2017.

Jonathan Krause, Michael Stark, Jia Deng, and Li Fei-Fei. 3d object representations for fine-grained categorization. In *Proceedings of the IEEE international conference on computer vision workshops*, 2013.

Alex Krizhevsky, Geoffrey Hinton, et al. Learning multiple layers of features from tiny images. 2009.

Lei Li, Yuqi Wang, Runxin Xu, et al. Multimodal arxiv: A dataset for improving scientific comprehension of large vision-language models. In *arXiv preprint arXiv:2403.00231*, 2024.

Zhizhong Li and Derek Hoiem. Learning without forgetting. *IEEE transactions on pattern analysis and machine intelligence*, 40(12):2935–2947, 2017.

Yan-Shuo Liang and Wu-Jun Li. Adaptive plasticity improvement for continual learning. In *Proceedings of the IEEE/CVF conference on computer vision and pattern recognition*, pp. 7816–7825, 2023.

Yan-Shuo Liang and Wu-Jun Li. Inflora: Interference-free low-rank adaptation for continual learning. In *Proceedings of the IEEE/CVF Conference on Computer Vision and Pattern Recognition*, pp. 23638–23647, 2024.

Adam Dahlgren Lindström and Savitha Sam Abraham. Clevr-math: A dataset for compositional language, visual and mathematical reasoning. In *arXiv preprint arXiv:2208.05358*, 2022.

Haotian Liu, Chunyuan Li, Qingyang Wu, and Yong Jae Lee. Visual instruction tuning. *Advances in neural information processing systems*, 36:34892–34916, 2023.

Sylvain Lobry, Diego Marcos, Jesse Murray, et al. Rsvqa: Visual question answering for remote sensing data. In *IEEE Transactions on Geoscience and Remote Sensing*, volume 58, pp. 8555–8566, 2020.

Ilya Loshchilov and Frank Hutter. Decoupled weight decay regularization. In *International Conference on Learning Representations (ICLR)*, 2019.

Pan Lu, Liang Qiu, Jiaqi Chen, Tony Xia, Yizhou Zhao, Wei Zhang, Zhou Yu, Xiaodan Liang, and Song-Chun Zhu. Iconqa: A new benchmark for abstract diagram understanding and visual language reasoning. In *Proceedings of the 35th Conference on Neural Information Processing Systems (NeurIPS) Track on Datasets and Benchmarks*, 2021.

Mao-Lin Luo, Zi-Hao Zhou, Tong Wei, and Min-Ling Zhang. Lada: Scalable label-specific clip adapter for continual learning. In *Forty-second International Conference on Machine Learning*, 2025.

Subhransu Maji, Esa Rahtu, Juho Kannala, Matthew Blaschko, and Andrea Vedaldi. Fine-grained visual classification of aircraft. *arXiv preprint arXiv:1306.5151*, 2013.

Jishnu Mukhoti, Yarin Gal, Philip Torr, and Puneet K. Dokania. Fine-tuning can cripple your foundation model; preserving features may be the solution. *Transactions on Machine Learning Research*, 2024. ISSN 2835-8856. Featured Certification.

Nikhil Shivakumar Nayak, Krishnateja Killamsetty, Ligong Han, Abhishek Bhandwaldar, Prateek Chanda, Kai Xu, Hao Wang, Aldo Pareja, Oleg Silkin, Mustafa Eyceoz, et al. Sculpting subspaces: Constrained full fine-tuning in llms for continual learning. *arXiv preprint arXiv:2504.07097*, 2025.

Maria-Elena Nilsback and Andrew Zisserman. Automated flower classification over a large number of classes. In *2008 Sixth Indian conference on computer vision, graphics & image processing*, 2008.

Omkar M Parkhi, Andrea Vedaldi, Andrew Zisserman, and CV Jawahar. Cats and dogs. In *2012 IEEE conference on computer vision and pattern recognition (CVPR)*, 2012.

Bryan A Plummer, Liwei Wang, Chris M Cervantes, Juan C Caicedo, Julia Hockenmaier, and Svetlana Lazebnik. Flickr30k entities: Collecting region-to-phrase correspondences for richer image-to-sentence models. In *Proceedings of the IEEE International Conference on Computer Vision (ICCV)*, pp. 2641–2649, 2015.

Jingyang Qiao, zhizhong zhang, Xin Tan, Chengwei Chen, Yanyun Qu, Yong Peng, and Yuan Xie. Prompt gradient projection for continual learning. In *The Twelfth International Conference on Learning Representations*, 2024.

Alec Radford, Jong Wook Kim, Chris Hallacy, Aditya Ramesh, Gabriel Goh, Sandhini Agarwal, Girish Sastry, Amanda Askell, Pamela Mishkin, Jack Clark, et al. Learning transferable visual models from natural language supervision. In *International conference on machine learning*, pp. 8748–8763. PmLR, 2021.

Sylvestre-Alvise Rebuffi, Alexander Kolesnikov, Georg Sperl, and Christoph H Lampert. icarl: Incremental classifier and representation learning. In *Proceedings of the IEEE conference on Computer Vision and Pattern Recognition*, pp. 2001–2010, 2017.

David Rolnick, Arun Ahuja, Jonathan Schwarz, Timothy Lillicrap, and Gregory Wayne. Experience replay for continual learning. *Advances in neural information processing systems*, 32, 2019.

Robin Rombach, Andreas Blattmann, Dominik Lorenz, Patrick Esser, and Björn Ommer. High-resolution image synthesis with latent diffusion models. In *Proceedings of the IEEE/CVF conference on computer vision and pattern recognition*, pp. 10684–10695, 2022.

Gobinda Saha, Isha Garg, and Kaushik Roy. Gradient projection memory for continual learning. In *International Conference on Learning Representations*, 2021.

Piyush Sharma, Nan Ding, Sebastian Goodman, and Radu Soricut. Conceptual captions: A cleaned, hypernymed, image alt-text dataset for automatic image captioning. In *Proceedings of the 56th Annual Meeting of the Association for Computational Linguistics (Volume 1: Long Papers)*, pp. 2556–2565, 2018.

Pratyusha Sharma, Jordan T. Ash, and Dipendra Misra. The truth is in there: Improving reasoning in language models with layer-selective rank reduction. In *The Twelfth International Conference on Learning Representations*, 2024.

Chonghao Sima, Katrin Renz, Kashyap Chitta, Li Chen, Hanxue Zhang, Chengen Xie, Jens Beißwenger, Ping Luo, Andreas Geiger, and Hongyang Li. Drivelm: Driving with graph visual question answering. In *European Conference on Computer Vision (ECCV)*, pp. 256–274. Springer, 2024.

James Seale Smith, Leonid Karlinsky, Vyshnavi Gutta, Paola Cascante-Bonilla, Donghyun Kim, Assaf Arbelle, Rameswar Panda, Rogerio Feris, and Zsolt Kira. Coda-prompt: Continual decomposed attention-based prompting for rehearsal-free continual learning. In *Proceedings of the IEEE/CVF conference on computer vision and pattern recognition*, pp. 11909–11919, 2023.

Longxiang Tang, Zhuotao Tian, Kai Li, Chunming He, Hantao Zhou, Hengshuang Zhao, Xiu Li, and Jiaya Jia. Mind the interference: Retaining pre-trained knowledge in parameter efficient continual learning of vision-language models. In *European conference on computer vision*, pp. 346–365. Springer, 2024.

Liyuan Wang, Xingxing Zhang, Hang Su, and Jun Zhu. A comprehensive survey of continual learning: Theory, method and application. *IEEE transactions on pattern analysis and machine intelligence*, 46(8):5362–5383, 2024.

Xiao Wang, Tianze Chen, Qiming Ge, Han Xia, Rong Bao, Rui Zheng, Qi Zhang, Tao Gui, and Xuan-Jing Huang. Orthogonal subspace learning for language model continual learning. In *Findings of the Association for Computational Linguistics: EMNLP 2023*, pp. 10658–10671, 2023a.

Yabin Wang, Zhiwu Huang, and Xiaopeng Hong. S-prompts learning with pre-trained transformers: An occam’s razor for domain incremental learning. *Advances in Neural Information Processing Systems*, 35:5682–5695, 2022a.

Ziao Wang, Yuhang Li, Junda Wu, Jaehyeon Soon, and Xiaofeng Zhang. Finvis-gpt: A multimodal large language model for financial chart analysis. In *arXiv preprint arXiv:2308.01430*, 2023b.

Zifeng Wang, Zizhao Zhang, Sayna Ebrahimi, Ruoxi Sun, Han Zhang, Chen-Yu Lee, Xiaoqi Ren, Guolong Su, Vincent Perot, Jennifer Dy, et al. Dualprompt: Complementary prompting for rehearsal-free continual learning. In *European conference on computer vision*, pp. 631–648. Springer, 2022b.

Zifeng Wang, Zizhao Zhang, Chen-Yu Lee, Han Zhang, Ruoxi Sun, Xiaoqi Ren, Guolong Su, Vincent Perot, Jennifer Dy, and Tomas Pfister. Learning to prompt for continual learning. In *Proceedings of the IEEE/CVF conference on computer vision and pattern recognition*, pp. 139–149, 2022c.

Mitchell Wortsman, Gabriel Ilharco, Jong Wook Kim, Mike Li, Simon Kornblith, Rebecca Roelofs, Raphael Gontijo Lopes, Hannaneh Hajishirzi, Ali Farhadi, Hongseok Namkoong, et al. Robust fine-tuning of zero-shot models. In *Proceedings of the IEEE/CVF conference on computer vision and pattern recognition*, pp. 7959–7971, 2022.

Bin Wu, Wuxuan Shi, Jinqiao Wang, and Mang Ye. Synthetic data is an elegant gift for continual vision-language models. In *Proceedings of the Computer Vision and Pattern Recognition Conference*, pp. 2813–2823, 2025a.

Yichen Wu, Hongming Piao, Long-Kai Huang, Renzhen Wang, Wanhua Li, Hanspeter Pfister, Deyu Meng, Kede Ma, and Ying Wei. Sd-lora: Scalable decoupled low-rank adaptation for class incremental learning. *arXiv preprint arXiv:2501.13198*, 2025b.

Jianxiong Xiao, James Hays, Krista A Ehinger, Aude Oliva, and Antonio Torralba. Sun database: Large-scale scene recognition from abbey to zoo. In *IEEE computer society conference on computer vision and pattern recognition*, 2010.

Jiazu Yu, Yunzhi Zhuge, Lu Zhang, Ping Hu, Dong Wang, Huchuan Lu, and You He. Boosting continual learning of vision-language models via mixture-of-experts adapters. In *Proceedings of the IEEE/CVF Conference on Computer Vision and Pattern Recognition*, pp. 23219–23230, 2024.

Ted Zadouri, Ahmet Üstün, Arash Ahmadian, Beyza Ermiş, Acyr Locatelli, and Sara Hooker. Pushing mixture of experts to the limit: Extremely parameter efficient moe for instruction tuning. *arXiv preprint arXiv:2309.05444*, 2023.

Hongbo Zhao, Fei Zhu, Rundong Wang, Gaofeng Meng, and Zhaoxiang Zhang. Mllm-cl: Continual learning for multimodal large language models. In *arXiv preprint arXiv:2506.05453*, 2025.

Zangwei Zheng, Mingyuan Ma, Kai Wang, Ziheng Qin, Xiangyu Yue, and Yang You. Preventing zero-shot transfer degradation in continual learning of vision-language models. In *Proceedings of the IEEE/CVF international conference on computer vision*, pp. 19125–19136, 2023.

Da-Wei Zhou, Qi-Wei Wang, Zhi-Hong Qi, Han-Jia Ye, De-Chuan Zhan, and Ziwei Liu. Class-incremental learning: A survey. *IEEE Transactions on Pattern Analysis and Machine Intelligence*, 46(12):9851–9873, 2024.

A PROOFS OF PROPOSITIONS

A.1 PROOFS OF PROPOSITION 3.1

Proof. Suppose for loss function \mathcal{L} for task \mathcal{T}^t and a linear layer with $\mathbf{y} = \mathbf{x}\mathbf{W}$, where \mathbf{y} is output of layer and \mathbf{x} is the input. We can compute gradient of \mathbf{B}_t directly as follow:

$$\frac{\partial \mathcal{L}}{\partial \mathbf{B}_t} = \frac{\partial \mathbf{W}}{\partial \mathbf{B}_t} \cdot \frac{\partial \mathcal{L}}{\partial \mathbf{W}} = \frac{\alpha}{r} \mathbf{A}_t^\top \mathbf{G}_t. \quad (9)$$

In a gradient descent iteration, the change of \mathbf{B}_t is represented by a negative gradient: $\Delta \mathbf{B}_t = -\frac{\eta\alpha}{r} \mathbf{A}_t^\top \mathbf{G}_t$. Therefore, when \mathbf{A}_t is frozen to only update \mathbf{B}_t in each iteration, we can obtain the variation of \mathbf{W} in one iteration to complete the proof:

$$\Delta \mathbf{W} = \frac{\alpha}{r} \mathbf{A}_t \Delta \mathbf{B}_t = -\frac{\eta\alpha^2}{r^2} \mathbf{A}_t \mathbf{A}_t^\top \mathbf{G}_t. \quad (10)$$

□

A.2 PROOFS OF PROPOSITION 3.2

Proof. We proceed by transforming the constrained optimization problem, leveraging subspace properties, and applying the Eckart–Young–Mirsky Theorem (Eckart & Young, 1936) to confirm the optimal solution.

Step 1: Equivalent Transformation of the Objective Function. For an orthonormal matrix \mathbf{A}_t satisfying $\mathbf{A}_t^\top \mathbf{A}_t = \mathbf{I}$, the orthogonal projection operator $\mathbf{P}_{\mathbf{A}_t} = \mathbf{A}_t \mathbf{A}_t^\top$ satisfies the Pythagorean theorem for the Frobenius norm:

$$\|\mathbf{G}_t\|_F^2 = \|\mathbf{P}_{\mathbf{A}_t} \mathbf{G}_t\|_F^2 + \|\mathbf{G}_t - \mathbf{P}_{\mathbf{A}_t} \mathbf{G}_t\|_F^2.$$

Since $\|\mathbf{G}_t\|_F^2$ is a constant independent of \mathbf{A}_t , minimizing the original objective $\|\mathbf{G}_t - \mathbf{P}_{\mathbf{A}_t} \mathbf{G}_t\|_F^2$ is equivalent to maximizing the projected norm $\|\mathbf{P}_{\mathbf{A}_t} \mathbf{G}_t\|_F^2$. The optimization problem thus can be rewritten as:

$$\begin{aligned} & \max_{\mathbf{A}_t^\top \mathbf{A}_t = \mathbf{I}} \|\mathbf{A}_t \mathbf{A}_t^\top \mathbf{G}_t\|_F^2, \\ \text{s.t. } & \mathbf{W}_p^\top \mathbf{A}_t = \mathbf{M}_{t-1}^\top \mathbf{A}_t = \mathbf{0}. \end{aligned} \quad (11)$$

Step 2: Substitute $\hat{\mathbf{G}}_t$ and Simplify Using Constraints. Recall from Eq. 5 that the projected gradient $\hat{\mathbf{G}}_t$ is defined as:

$$\hat{\mathbf{G}}_t = \mathbf{G}_t - \mathbf{W}_p \mathbf{W}_p^\top \mathbf{G}_t - \mathbf{M}_{t-1} \mathbf{M}_{t-1}^\top \mathbf{G}_t.$$

Rearranging gives $\mathbf{G}_t = \hat{\mathbf{G}}_t + \mathbf{W}_p \mathbf{W}_p^\top \mathbf{G}_t + \mathbf{M}_{t-1} \mathbf{M}_{t-1}^\top \mathbf{G}_t$. Substitute this into the objective:

$$\|\mathbf{A}_t \mathbf{A}_t^\top (\hat{\mathbf{G}}_t + \mathbf{W}_p \mathbf{W}_p^\top \mathbf{G}_t + \mathbf{M}_{t-1} \mathbf{M}_{t-1}^\top \mathbf{G}_t)\|_F^2.$$

For any feasible \mathbf{A}_t , we use $\mathbf{W}_p^\top \mathbf{A}_t = \mathbf{M}_{t-1}^\top \mathbf{A}_t = \mathbf{0}$ to simplify: $\mathbf{A}_t^\top (\mathbf{W}_p \mathbf{W}_p^\top \mathbf{G}_t) = (\mathbf{W}_p^\top \mathbf{A}_t)^\top (\mathbf{W}_p^\top \mathbf{G}_t) = \mathbf{0}^\top (\mathbf{W}_p^\top \mathbf{G}_t) = \mathbf{0}$. Similarly, $\mathbf{A}_t^\top (\mathbf{M}_{t-1} \mathbf{M}_{t-1}^\top \mathbf{G}_t) = \mathbf{0}$.

Thus, $\mathbf{A}_t \mathbf{A}_t^\top (\mathbf{W}_p \mathbf{W}_p^\top \mathbf{G}_t + \mathbf{M}_{t-1} \mathbf{M}_{t-1}^\top \mathbf{G}_t) = \mathbf{0}$, and the objective reduces to maximizing $\|\mathbf{A}_t \mathbf{A}_t^\top \hat{\mathbf{G}}_t\|_F^2$. The optimization problem simplifies to:

$$\begin{aligned} & \max_{\mathbf{A}_t^\top \mathbf{A}_t = \mathbf{I}} \|\mathbf{A}_t \mathbf{A}_t^\top \hat{\mathbf{G}}_t\|_F^2, \\ \text{s.t. } & \mathbf{W}_p^\top \mathbf{A}_t = \mathbf{M}_{t-1}^\top \mathbf{A}_t = \mathbf{0}. \end{aligned} \quad (12)$$

Step 3: Optimal \mathbf{A}_t via Eckart–Young–Mirsky Theorem. The Eckart–Young–Mirsky Theorem (Eckart & Young, 1936) states that for any matrix $\mathbf{X} \in \mathbb{R}^{m \times n}$ and integer $k \leq \min(m, n)$, the r -dimensional subspace that maximizes $\|\mathbf{P}\mathbf{X}\|_F^2$, where \mathbf{P} is the orthogonal projection onto the subspace, is spanned by the top- r left singular vectors of \mathbf{X} .

Here, $\mathbf{X} = \hat{\mathbf{G}}_t$, and we seek an r -dimensional subspace spanned by \mathbf{A}_t to maximize $\|\mathbf{A}_t \mathbf{A}_t^\top \hat{\mathbf{G}}_t\|_F^2$. By the theorem, the optimal \mathbf{A}_t consists of the top- r left singular vectors of $\hat{\mathbf{G}}_t$.

Step 4: Verify Feasibility of the Optimal \mathbf{A}_t . We confirm the optimal \mathbf{A}_t satisfies the constraints $\mathbf{W}_p^\top \mathbf{A}_t = \mathbf{0}$ and $\mathbf{M}_{t-1}^\top \mathbf{A}_t = \mathbf{0}$.

By the definition of $\hat{\mathbf{G}}_t$ in Eq. 5, we have:

$$\mathbf{W}_p^\top \hat{\mathbf{G}}_t = \mathbf{0}, \quad \mathbf{M}_{t-1}^\top \hat{\mathbf{G}}_t = \mathbf{0}. \quad (13)$$

Substituting SVD of $\hat{\mathbf{G}} = \mathbf{U} \mathbf{S} \mathbf{V}$ in Eq. 13 : $\mathbf{W}_p^\top \hat{\mathbf{G}}_t = \mathbf{W}_p^\top \mathbf{U} \mathbf{S} \mathbf{V}^\top = \mathbf{0}$. Since $\mathbf{S} \mathbf{V}^\top$ is column-full rank (singular values are non-negative, and \mathbf{V} is orthonormal), $\mathbf{W}_p^\top \mathbf{U}$ must be the zero matrix. Thus, $\mathbf{W}_p^\top \mathbf{U} = \mathbf{0}$, hence $\mathbf{W}_p^\top \mathbf{A}_t = \mathbf{W}_p^\top \mathbf{U}_{:,1:r} = \mathbf{0}$. The same logic applies to \mathbf{M}_{t-1} : $\mathbf{M}_{t-1}^\top \hat{\mathbf{G}}_t = \mathbf{M}_{t-1}^\top \mathbf{U} \mathbf{S} \mathbf{V}^\top = \mathbf{0}$ implies $\mathbf{M}_{t-1}^\top \mathbf{U} = \mathbf{0}$, hence $\mathbf{M}_{t-1}^\top \mathbf{A}_t = \mathbf{0}$.

Thus, the optimal solution to Eq. 8 is exactly the top- r left singular vectors of $\hat{\mathbf{G}}_t$, which matches KeepLoRA \mathbf{A}_t initialization. The proof is completed. \square

B EXPERIMENT DETAILS

B.1 BENCHMARK

MTIL benchmark (Zheng et al., 2023) consists of 11 image classification datasets: Aircraft (Maji et al., 2013), Caltech101 (Fei-Fei et al., 2004), Cifar100 (Krizhevsky et al., 2009), DTD (Cimpoi et al., 2014), EuroSAT (Helber et al., 2019), Flowers (Nilsback & Zisserman, 2008), Food (Bossard et al., 2014), MNIST (Deng, 2012), OxfordPet (Parkhi et al., 2012), StanfordCars (Krause et al., 2013), and SUN397 (Xiao et al., 2010). Each dataset is treated as a task.

MLLM-DCL benchmark (Zhao et al., 2025) consists of multiple downstream VQA datasets: RSVQA (Lobry et al., 2020), PathVQA (He et al., 2020), DriveLM (Sima et al., 2024), FinVis (Wang et al., 2023b), AI2D (Kembhavi et al., 2016), Sciverse (Guo et al., 2025c), MapQA (Chang et al., 2022), and TQA (Kembhavi et al., 2017). It covers 5 specialized areas: Remote Sensing, Medical, Driving, Finance, and Science. Each area is treated as a task.

UCIT benchmark (Guo et al., 2025a) consists of 6 VQA datasets: ArxivQA (Li et al., 2024), CLEVR-Math (Lindström & Abraham, 2022), IconQA (Lu et al., 2021), ImageNet-R (Hendrycks et al., 2021), VizWiz-Caption (Gurari et al., 2018), and Flickr30k (Plummer et al., 2015). Each dataset is treated as a task.

B.2 EVALUATION METRICS

We define the *Transfer*, *Average*, and *Last* metrics to evaluate model performance under continual learning scenarios. Let $a_t^{(i)}$ represent the accuracy of the model on task t after training on task i with a total of n tasks. The *Transfer*, *Average*, and *Last* metrics for task t are computed as follows:

$$\text{Transfer}_t = \frac{1}{t-1} \sum_{i=1}^{t-1} a_t^{(i)}, \quad t = 2, 3, \dots, n, \quad (14)$$

$$\text{Average}_t = \frac{1}{n} \sum_{i=1}^n a_t^{(i)}, \quad t = 1, 2, \dots, n, \quad (15)$$

$$\text{Last}_t = a_t^{(n)}, \quad t = 1, 2, \dots, n. \quad (16)$$

The *Transfer* metric evaluates forward stability by measuring the performance of unseen tasks throughout $(i+1, i+2, \dots, n)$ after training on the task i . The *Last* metric measures the final performance on each task after completing all training steps, quantifying both plasticity and backward stability. The *Average* metric represents the mean accuracy across all time steps, offering a holistic measure of stability and plasticity.

B.3 IMPLEMENTATION DETAILS OF KEEPLORA+

We extend KeepLoRA with a structure variant, termed KeepLoRA+, which incorporates a prototype vector for each class name to improve classification performance. Each prototype vector is initialized using the mean feature extracted by the vision encoder from the corresponding class samples. During the training stage, we jointly optimize the prototype vectors alongside the KeepLoRA parameters. In the inference stage, the logits derived from the similarity of the prototype vectors are averaged with the logits calculated from the text-side contrast.

B.4 ADDITIONAL IMPLEMENTATION DETAILS

CLIP Experiments. We adopt the CLIP (Radford et al., 2021) model with a ViT-B/16 (Dosovitskiy et al., 2021) image encoder. The training process is carried out using the AdamW (Loshchilov & Hutter, 2019) optimizer, with a learning rate of 10^{-3} and a batch size of 64 across all tasks with no more than 10 epochs. For the primary experiments, we set the hyperparameters as $\epsilon_{w(\text{vision})} = 0.85$ and $\epsilon_{w(\text{text})} = 0.2$ in vision encoder and text encoder separately and set $\epsilon_f = 0.99$. KeepLoRA+ is a structure extension variant with an extension prototype vector for a classname to help classification. All experiments of KeepLoRA are conducted on a single NVIDIA 4090 GPU. For the reproduced methods, we performed careful hyperparameter tuning. For O-LoRA (Wang et al., 2023a), the learning rate is 5×10^{-4} with a regularization coefficient of 0.1. For InfLoRA (Liang & Li, 2024), the learning rate is 10^{-3} , with $\epsilon_f = 0.99$. The learning rate for SD-LoRA (Wu et al., 2025b) is set to 5×10^{-3} .

LLaVA Experiments. We adopt the LLaVA-1.5-7b (Liu et al., 2023) model for multimodal continual instruction tuning experiments. The training is conducted on $4 \times$ NVIDIA H100 GPUs using the AdamW optimizer. For the MLLM-DCL benchmark, we set the learning rate to 2×10^{-5} and train for no more than 3 epochs per task. For the UCIT benchmark, the learning rate is set to 2×10^{-4} for all tasks except Flickr30k, which uses 1×10^{-4} and train 1 epoch for each task. The hyperparameters for subspace constraints are configured as $\epsilon_w = 0.6$ and $\epsilon_f = 0.99$.

C SUPPLEMENTARY EXPERIMENTS

C.1 COMPARISON ON MTIL WITH ORDER II.

We compare different methods on MTIL in random order: StanfordCars, Food, MNIST, OxfordPet, Flowers, SUN397, Aircraft, Caltech101, DTD, EuroSAT and CIFAR100. As shown in Tab. 6, KeepLoRA consistently outperforms previous methods across all metrics.

C.2 HYPERPARAMETER ANALYSIS

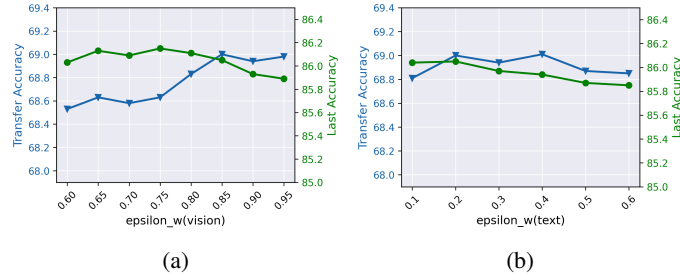


Figure 4: Effects of hyperparameters $\epsilon_{w(\text{vision})}$ and $\epsilon_{w(\text{text})}$ on *Transfer* and *Last*, respectively.

We examine the effects of hyperparameters $\epsilon_{w(\text{vision})}$ and $\epsilon_{w(\text{text})}$ on *Transfer* and *Last*. For the image encoder, *Last* fluctuates slightly, with a minor decline when $\epsilon_{w(\text{vision})}$ is larger. Between 0.75 and 0.85, *Transfer* shows a clear increase. For the text encoder, which uses only class names and thus has much less training data than images, the coefficient $\epsilon_{w(\text{text})}$ exhibits low performance sensitivity. Datasets with image-text pairs or VQA tasks, which include substantial text data, warrant further study in this regard.

Table 6: Comparison of different continual learning methods on MTIL for each task with order-II in terms of *Transfer*, *Average*, and *Last* scores (%). The best results are highlighted with **bold** style.

| Method | Inf. | Efficiency | w/o Extra Data | Cars | Food | MNIST | Oxfordpet | Flowers | Sun397 | Aircraft | Caltech101 | DTD | EuroSAT | CIFAR100 | Avg. |
|---------------------------------|------|------------|----------------|-------------|-------------|-------------|-------------|-------------|-------------|-------------|-------------|-------------|-------------|-------------|------|
| Zero-shot | ✓ | ✓ | 64.7 | 88.5 | 59.4 | 89.0 | 71.0 | 65.4 | 24.8 | 88.4 | 44.6 | 54.9 | 68.2 | | |
| Transfer | | | | | | | | | | | | | | | |
| LwF (Li & Hoiem, 2017) | ✓ | ✗ | — | 87.8 | 58.5 | 71.9 | 46.6 | 57.3 | 12.8 | 81.4 | 34.5 | 34.5 | 46.8 | 53.2 | |
| iCaRL (Rebuffi et al., 2017) | ✓ | ✗ | — | 86.1 | 51.8 | 67.6 | 50.4 | 57.9 | 11.0 | 72.3 | 31.2 | 32.7 | 48.1 | 50.9 | |
| LwF-VR (Ding et al., 2022) | ✓ | ✗ | — | 88.2 | 57.0 | 71.4 | 50.0 | 58.0 | 13.0 | 82.0 | 34.4 | 29.3 | 47.6 | 53.1 | |
| WiSE-FT (Wortsman et al., 2022) | ✓ | ✗ | — | 87.2 | 57.6 | 67.0 | 45.0 | 54.0 | 12.9 | 78.6 | 35.5 | 28.4 | 44.3 | 51.1 | |
| ZSCL (Zheng et al., 2023) | ✓ | ✗ | — | <u>88.3</u> | 57.5 | 84.7 | 68.1 | 64.8 | 21.1 | <u>88.2</u> | <u>45.3</u> | 55.2 | <u>68.2</u> | <u>64.1</u> | |
| O-LoRA (Wang et al., 2023a) | ✓ | ✓ | — | 87.8 | 56.7 | 90.1 | <u>71.4</u> | 64.0 | 20.7 | 87.4 | 43.9 | 46.3 | 65.9 | 63.4 | |
| InfLoRA (Liang & Li, 2024) | ✓ | ✓ | — | 88.2 | 56.7 | 90.2 | 71.3 | 65.0 | 22.2 | 88.2 | 43.8 | 47.3 | 67.2 | 64.0 | |
| SD-LoRA (Wu et al., 2025b) | ✓ | ✓ | — | 88.0 | 56.4 | <u>90.5</u> | 71.0 | 64.6 | 22.0 | 87.8 | 43.7 | 47.1 | 66.4 | 63.7 | |
| KeepLoRA | ✓ | ✓ | — | 88.7 | <u>57.7</u> | 91.2 | 72.1 | 65.8 | 23.4 | 88.8 | 45.4 | <u>48.5</u> | 68.2 | 65.0 | |
| L2P (Wang et al., 2022c) | ✗ | ✓ | — | 70.6 | 30.7 | 78.3 | 42.8 | 38.3 | 17.4 | 75.3 | 27.4 | 23.1 | 20.7 | 42.5 | |
| DualPrompt (Wang et al., 2022b) | ✗ | ✓ | — | 79.9 | 46.9 | 85.2 | 51.3 | 45.1 | 9.3 | 82.7 | 29.9 | 42.9 | 47.2 | 52.1 | |
| S-Prompts (Wang et al., 2022a) | ✗ | ✓ | — | 59.8 | 46.2 | 67.7 | 47.5 | 43.8 | 13.5 | 76.8 | 31.4 | 22.6 | 43.5 | 45.3 | |
| DIKI (Tang et al., 2024) | ✗ | ✓ | — | 85.8 | 59.8 | <u>89.1</u> | <u>71.8</u> | 62.6 | <u>24.3</u> | <u>93.3</u> | 42.7 | 46.8 | 67.8 | 64.4 | |
| MoE-Adapters (Yu et al., 2024) | ✗ | ✗ | — | <u>88.8</u> | <u>59.5</u> | <u>89.1</u> | 69.9 | <u>64.4</u> | 18.1 | 86.9 | 43.7 | 54.6 | 68.2 | 64.3 | |
| IAP (Fu et al., 2025) | ✗ | ✓ | — | 85.7 | 59.4 | <u>89.1</u> | 71.3 | 62.7 | 24.4 | 94.0 | 43.8 | 49.0 | 68.6 | 64.9 | |
| KeepLoRA+ | ✗ | ✓ | — | 89.1 | 58.1 | 90.7 | 72.4 | 65.4 | 24.0 | 88.9 | 44.0 | <u>52.7</u> | 70.2 | 65.5 | |
| Average | | | | | | | | | | | | | | | |
| LwF (Li & Hoiem, 2017) | ✓ | ✗ | 49.0 | 77.0 | 92.1 | 85.9 | 66.5 | 67.2 | 20.9 | 84.7 | 44.6 | 45.5 | 50.5 | 62.2 | |
| iCaRL (Rebuffi et al., 2017) | ✓ | ✗ | 52.0 | 75.9 | 77.4 | 74.6 | 58.4 | 59.3 | 11.7 | 79.6 | 42.1 | 43.2 | 51.7 | 56.9 | |
| LwF-VR (Ding et al., 2022) | ✓ | ✗ | 44.9 | 75.8 | 91.8 | 85.3 | 63.5 | 67.6 | 16.9 | 84.9 | 44.0 | 40.6 | 51.3 | 60.6 | |
| WiSE-FT (Wortsman et al., 2022) | ✓ | ✗ | 52.6 | 79.3 | 91.9 | 83.9 | 63.4 | 65.2 | 23.3 | 83.7 | 45.4 | 40.0 | 48.2 | 61.5 | |
| ZSCL (Zheng et al., 2023) | ✓ | ✗ | 81.7 | 91.3 | 91.9 | 91.0 | <u>82.9</u> | 72.5 | 33.6 | 89.7 | 53.3 | 62.8 | <u>69.9</u> | <u>74.6</u> | |
| O-LoRA (Wang et al., 2023a) | ✓ | ✓ | 78.5 | 91.0 | 91.3 | 92.3 | 77.7 | 73.0 | 33.5 | 90.5 | 50.7 | 55.1 | 67.8 | 72.9 | |
| InfLoRA (Liang & Li, 2024) | ✓ | ✓ | <u>84.0</u> | <u>92.1</u> | 91.7 | <u>93.2</u> | 81.6 | <u>74.3</u> | <u>34.3</u> | <u>91.3</u> | 51.5 | 56.6 | 69.0 | 74.5 | |
| SD-LoRA (Wu et al., 2025b) | ✓ | ✓ | 76.8 | 91.1 | 90.8 | 92.5 | 76.5 | 73.1 | 34.0 | 90.7 | 49.1 | 56.2 | 68.2 | 72.6 | |
| KeepLoRA | ✓ | ✓ | 85.2 | 92.3 | <u>92.0</u> | 93.7 | 84.8 | 74.8 | 35.9 | 91.8 | 53.1 | <u>57.5</u> | 70.0 | 75.6 | |
| L2P (Wang et al., 2022c) | ✗ | ✓ | 80.1 | 87.4 | 86.7 | 89.6 | 76.8 | 59.1 | 27.7 | 79.5 | 39.9 | 34.6 | 26.5 | 62.5 | |
| DualPrompt (Wang et al., 2022b) | ✗ | ✓ | 78.6 | 88.4 | 89.7 | 91.7 | 80.0 | 62.4 | 23.2 | 85.0 | 41.3 | 51.6 | 50.7 | 67.5 | |
| S-Prompts (Wang et al., 2022a) | ✗ | ✓ | 79.2 | 86.5 | 89.5 | 87.0 | 78.2 | 61.5 | 25.5 | 83.6 | 41.9 | 36.3 | 47.2 | 65.1 | |
| DIKI (Tang et al., 2024) | ✗ | ✓ | 81.9 | 88.9 | 92.1 | 92.8 | <u>87.7</u> | 70.3 | <u>34.3</u> | <u>94.2</u> | 51.5 | 56.1 | 69.5 | 74.5 | |
| MoE-Adapters (Yu et al., 2024) | ✗ | ✗ | <u>84.9</u> | <u>89.9</u> | 89.3 | 91.4 | 86.2 | <u>72.2</u> | 33.4 | 89.4 | 53.3 | 61.4 | 69.9 | 74.7 | |
| IAP (Fu et al., 2025) | ✗ | ✓ | 82.5 | 89.2 | 92.3 | <u>93.2</u> | 88.0 | 70.4 | <u>34.3</u> | 94.4 | 52.4 | 57.9 | 70.2 | 75.1 | |
| KeepLoRA+ | ✗ | ✓ | 88.0 | 92.4 | 91.9 | 93.9 | 87.4 | 75.2 | 39.2 | 92.0 | 52.8 | 60.9 | 71.8 | 76.9 | |
| Last | | | | | | | | | | | | | | | |
| LwF (Li & Hoiem, 2017) | ✓ | ✗ | 34.6 | 69.6 | 99.3 | 88.7 | 61.1 | 72.5 | 32.5 | 88.1 | 65.6 | 90.9 | 87.9 | 71.9 | |
| iCaRL (Rebuffi et al., 2017) | ✓ | ✗ | 46.0 | 81.5 | 91.3 | 82.8 | 66.5 | 72.2 | 16.3 | 91.6 | 68.1 | 83.2 | 87.8 | 71.6 | |
| LwF-VR (Ding et al., 2022) | ✓ | ✗ | 27.4 | 61.2 | 99.4 | 86.3 | 60.6 | 70.7 | 23.4 | 88.0 | 61.3 | 84.3 | 88.1 | 68.2 | |
| WiSE-FT (Wortsman et al., 2022) | ✓ | ✗ | 35.6 | 76.9 | 99.5 | 89.1 | 62.1 | 71.8 | 27.8 | 90.8 | 67.0 | 85.6 | 87.6 | 72.2 | |
| ZSCL (Zheng et al., 2023) | ✓ | ✗ | 78.2 | 91.1 | 97.6 | 92.5 | <u>87.4</u> | 78.2 | 45.0 | 92.3 | 72.7 | 96.2 | 86.3 | 83.4 | |
| O-LoRA (Wang et al., 2023a) | ✓ | ✓ | 70.3 | 89.8 | 97.8 | 92.9 | 73.8 | 79.8 | 44.4 | 95.3 | 66.3 | 91.5 | 85.9 | 80.7 | |
| InfLoRA (Liang & Li, 2024) | ✓ | ✓ | <u>82.4</u> | <u>92.0</u> | 99.3 | <u>93.9</u> | 85.4 | <u>81.2</u> | <u>46.1</u> | <u>96.5</u> | 70.0 | <u>97.6</u> | 87.2 | <u>84.7</u> | |
| SD-LoRA (Wu et al., 2025b) | ✓ | ✓ | 72.3 | 89.7 | 97.3 | 92.4 | 76.1 | 78.9 | 45.3 | 95.2 | 61.6 | 96.9 | 86.1 | 81.1 | |
| KeepLoRA | ✓ | ✓ | 83.7 | 92.2 | 99.5 | 94.4 | 90.7 | 81.3 | 49.0 | 96.9 | <u>72.3</u> | 98.0 | 87.3 | 85.9 | |
| L2P (Wang et al., 2022c) | ✗ | ✓ | 80.1 | 89.1 | 99.1 | 93.8 | 96.2 | 76.5 | 40.1 | 86.9 | 73.5 | 86.3 | 84.2 | 82.3 | |
| DualPrompt (Wang et al., 2022b) | ✗ | ✓ | 78.6 | <u>89.3</u> | 99.2 | 94.1 | 96.5 | 76.8 | 39.8 | 89.0 | 71.6 | 90.7 | 84.9 | 82.8 | |
| S-Prompts (Wang et al., 2022a) | ✗ | ✓ | 79.2 | 89.1 | 99.1 | 94.3 | 95.8 | 76.3 | 39.9 | 95.5 | 70.1 | 97.6 | 84.4 | 83.8 | |
| DIKI (Tang et al., 2024) | ✗ | ✓ | 81.9 | 89.2 | 99.4 | 94.3 | <u>96.8</u> | 76.7 | 46.3 | 95.9 | 74.8 | 98.3 | <u>86.6</u> | 85.5 | |
| MoE-Adapters (Yu et al., 2024) | ✗ | ✗ | <u>84.1</u> | 88.5 | 94.0 | 91.8 | 94.1 | <u>77.8</u> | <u>50.4</u> | 93.3 | 77.1 | 87.7 | <u>86.6</u> | 84.1 | |
| IAP (Fu et al., 2025) | ✗ | ✓ | 82.5 | 88.6 | 99.4 | <u>94.9</u> | 97.7 | 76.9 | 46.1 | <u>96.1</u> | 74.7 | 98.0 | <u>86.6</u> | <u>85.9</u> | |
| KeepLoRA+ | ✗ | ✓ | 87.4 | 92.5 | <u>99.3</u> | 95.0 | 96.0 | 83.2 | 56.9 | 97.5 | 76.9 | <u>98.0</u> | 88.0 | 88.2 | |

C.3 PER-TRAINING-STEP RESULTS

We present the detailed per-training-step accuracies through all training steps in Tab. 7, 8, 9, 10, 11 and 12. These results demonstrate strong performance in terms of both learning plasticity and stability.

Table 7: Accuracy of KeepLoRA on the MTIL benchmark with order-I. Each row represents the performance on every dataset of the model trained after the corresponding task. Transfer, Average, and Last metrics are shown.

| | Aircraft | Caltech101 | CIFAR100 | DTD | EuroSAT | Flowers | Food | MNIST | Oxfordpet | Cars | Sun397 | |
|------------|----------|------------|----------|------|---------|---------|------|-------|-----------|------|--------|------|
| Transfer | 84.6 | 68.7 | 45.9 | 54.3 | 70.1 | 87.7 | 64.8 | 90.3 | 59.5 | 64.1 | 69.0 | |
| Aircraft | 59.0 | 84.6 | 68.4 | 45.4 | 52.2 | 71.9 | 89.0 | 63.8 | 91.1 | 60.6 | 63.6 | |
| Caltech101 | 58.1 | 97.0 | 69.1 | 45.4 | 50.8 | 71.1 | 88.7 | 61.8 | 91.1 | 60.1 | 64.8 | |
| CIFAR100 | 56.0 | 96.8 | 87.6 | 46.8 | 56.3 | 68.9 | 87.3 | 66.3 | 90.1 | 59.6 | 64.7 | |
| DTD | 55.9 | 96.7 | 87.5 | 75.0 | 57.9 | 69.6 | 87.1 | 64.7 | 90.3 | 59.5 | 64.6 | |
| EuroSAT | 55.7 | 96.7 | 87.0 | 74.8 | 98.4 | 69.3 | 87.0 | 65.2 | 90.2 | 59.1 | 64.6 | |
| Flowers | 55.6 | 97.0 | 86.9 | 74.4 | 98.4 | 93.3 | 86.9 | 65.0 | 90.3 | 59.4 | 64.3 | |
| Food | 54.7 | 96.8 | 86.2 | 72.6 | 98.3 | 92.2 | 91.8 | 66.7 | 89.8 | 59.0 | 63.8 | |
| MNIST | 54.3 | 96.7 | 85.8 | 72.4 | 98.1 | 91.8 | 91.8 | 99.5 | 89.7 | 59.3 | 63.8 | |
| OxfordPet | 54.6 | 96.7 | 85.7 | 72.0 | 98.2 | 91.8 | 91.8 | 99.5 | 94.7 | 59.2 | 63.8 | |
| Cars | 54.2 | 96.7 | 85.7 | 71.9 | 98.1 | 91.5 | 91.7 | 99.5 | 94.4 | 84.3 | 63.7 | |
| SUN397 | 53.2 | 96.8 | 85.7 | 71.4 | 98.1 | 90.8 | 91.4 | 99.6 | 94.5 | 83.1 | 82.0 | 86.1 |
| Average | 55.6 | 95.7 | 83.2 | 65.6 | 82.2 | 82.0 | 89.5 | 77.4 | 91.5 | 63.9 | 65.8 | 77.5 |

Table 8: Accuracy of KeepLoRA on the MTIL benchmark with order-II. Each row represents the performance on every dataset of the model trained after the corresponding task. Transfer, Average, and Last metrics are shown.

| | Cars | Food | MNIST | OxfordPet | Flowers | Sun397 | Aircraft | Caltech101 | DTD | EuroSAT | CIFAR100 | |
|------------|------|------|-------|-----------|---------|--------|----------|------------|------|---------|----------|------|
| Transfer | 88.7 | 57.7 | 91.2 | 72.1 | 65.8 | 23.4 | 88.8 | 45.4 | 48.5 | 68.2 | 65.0 | |
| Cars | 86.2 | 88.7 | 57.1 | 91.3 | 71.7 | 65.5 | 23.5 | 87.4 | 46.6 | 50.7 | 69.5 | |
| Food | 85.9 | 92.9 | 58.3 | 91.1 | 72.3 | 66.0 | 23.9 | 88.3 | 45.3 | 49.8 | 70.5 | |
| MNIST | 85.8 | 92.8 | 99.6 | 91.2 | 71.9 | 66.2 | 23.0 | 88.6 | 46.4 | 50.4 | 68.1 | |
| OxfordPet | 85.7 | 92.8 | 99.6 | 94.8 | 72.4 | 65.9 | 23.0 | 89.3 | 46.0 | 48.2 | 67.8 | |
| Flowers | 85.6 | 92.8 | 99.6 | 94.8 | 92.4 | 65.7 | 23.0 | 89.3 | 46.2 | 46.9 | 67.5 | |
| Sun397 | 85.2 | 92.7 | 99.6 | 94.6 | 92.2 | 82.7 | 24.0 | 89.6 | 44.2 | 47.0 | 68.0 | |
| Aircraft | 84.8 | 92.7 | 99.6 | 94.6 | 92.1 | 82.7 | 51.6 | 89.3 | 44.2 | 46.3 | 68.0 | |
| Caltech101 | 84.8 | 92.7 | 99.6 | 94.6 | 92.2 | 82.6 | 51.6 | 97.1 | 44.5 | 48.7 | 68.3 | |
| DTD | 84.8 | 92.6 | 99.6 | 94.8 | 92.2 | 82.6 | 51.3 | 96.9 | 74.5 | 48.2 | 68.2 | |
| EuroSAT | 84.6 | 92.7 | 99.6 | 94.6 | 92.1 | 82.2 | 51.1 | 97.0 | 74.5 | 98.6 | 66.6 | |
| CIFAR100 | 83.7 | 92.3 | 99.5 | 94.4 | 90.8 | 81.3 | 49.0 | 96.9 | 72.3 | 98.0 | 87.3 | 85.9 |
| Average | 85.2 | 92.3 | 92.0 | 93.7 | 84.8 | 74.8 | 35.9 | 91.8 | 53.1 | 57.5 | 70.0 | 75.6 |

USE OF LARGE LANGUAGE MODELS

We use the large language model to polish text and check grammar. All outputs were reviewed by the authors, who take full responsibility for the final content.

Table 9: Accuracy of KeepLoRA+ on the MTIL benchmark with order-I. Each row represents the performance on every dataset of the model trained after the corresponding task. **Transfer**, **Average**, and **Last** metrics are shown.

| | Aircraft | Caltech101 | CIFAR100 | DTD | EuroSAT | Flowers | Food | MNIST | Oxfordpet | Cars | Sun397 |
|------------|----------|------------|----------|------|---------|---------|------|-------|-----------|------|--------|
| Transfer | 85.9 | 69.9 | 44.6 | 53.7 | 70.9 | 88.9 | 65.4 | 90.8 | 63.0 | 66.1 | 69.9 |
| Aircraft | 59.2 | 85.9 | 69.6 | 44.4 | 54.3 | 72.4 | 89.5 | 62.7 | 91.2 | 63.8 | 64.5 |
| Caltech101 | 59.2 | 97.5 | 70.2 | 44.3 | 53.3 | 71.4 | 89.5 | 62.7 | 91.4 | 63.8 | 65.1 |
| CIFAR100 | 59.0 | 97.8 | 88.2 | 45.1 | 52.7 | 70.3 | 88.7 | 67.8 | 90.8 | 63.3 | 66.3 |
| DTD | 59.0 | 97.8 | 88.0 | 76.4 | 54.4 | 70.5 | 88.6 | 66.6 | 90.7 | 63.3 | 66.3 |
| EuroSAT | 58.6 | 97.6 | 87.8 | 76.2 | 98.5 | 70.2 | 88.5 | 66.0 | 91.0 | 63.1 | 66.5 |
| Flowers | 58.8 | 97.6 | 87.9 | 76.1 | 98.5 | 95.8 | 88.4 | 66.4 | 90.8 | 63.1 | 66.4 |
| Food | 58.4 | 97.6 | 87.6 | 76.6 | 98.4 | 95.8 | 92.9 | 65.4 | 90.4 | 62.5 | 66.5 |
| MNIST | 57.8 | 97.6 | 87.3 | 76.8 | 98.4 | 95.9 | 92.9 | 99.5 | 90.2 | 62.2 | 66.5 |
| OxfordPet | 57.8 | 97.6 | 87.2 | 76.5 | 98.4 | 95.8 | 92.9 | 99.5 | 94.8 | 62.2 | 66.4 |
| Cars | 57.7 | 97.5 | 87.3 | 76.7 | 98.4 | 95.6 | 92.9 | 99.5 | 94.8 | 87.7 | 66.3 |
| SUN397 | 57.3 | 97.6 | 87.2 | 76.5 | 98.4 | 95.7 | 92.6 | 99.5 | 94.7 | 87.2 | 83.2 |
| Average | 58.4 | 96.5 | 84.4 | 67.8 | 82.1 | 84.5 | 90.7 | 77.8 | 91.9 | 67.5 | 67.6 |
| | | | | | | | | | | | 88.2 |

Table 10: Accuracy of KeepLoRA+ on the MTIL benchmark with order-II. Each row represents the performance on every dataset of the model trained after the corresponding task. **Transfer**, **Average**, and **Last** metrics are shown.

| | Cars | Food | MNIST | OxfordPet | Flowers | Sun397 | Aircraft | Caltech101 | DTD | EuroSAT | CIFAR100 |
|------------|------|------|-------|-----------|---------|--------|----------|------------|------|---------|----------|
| Transfer | 89.1 | 58.1 | 90.7 | 72.4 | 65.4 | 24.0 | 88.9 | 44.0 | 52.7 | 70.2 | 65.5 |
| Cars | 88.4 | 89.1 | 58.9 | 91.6 | 72.3 | 65.3 | 24.2 | 88.0 | 44.8 | 53.9 | 70.1 |
| Food | 88.3 | 92.8 | 57.2 | 90.1 | 72.4 | 65.4 | 24.2 | 88.5 | 44.5 | 52.5 | 70.8 |
| MNIST | 88.1 | 92.8 | 99.4 | 90.4 | 72.1 | 65.5 | 24.1 | 88.5 | 44.4 | 52.9 | 70.1 |
| OxfordPet | 88.3 | 92.7 | 99.4 | 95.2 | 72.8 | 65.3 | 24.1 | 88.7 | 44.2 | 52.2 | 70.2 |
| Flowers | 88.3 | 92.8 | 99.5 | 95.2 | 96.1 | 65.3 | 23.9 | 88.7 | 44.4 | 51.7 | 69.9 |
| Sun397 | 87.9 | 92.7 | 99.4 | 95.0 | 96.1 | 83.5 | 23.6 | 89.9 | 43.4 | 52.8 | 70.2 |
| Aircraft | 87.9 | 92.7 | 99.4 | 95.0 | 96.1 | 83.5 | 57.8 | 90.1 | 43.1 | 52.8 | 70.2 |
| Caltech101 | 87.7 | 92.7 | 99.4 | 95.0 | 96.0 | 83.5 | 57.5 | 97.4 | 43.0 | 52.6 | 70.4 |
| DTD | 87.7 | 92.7 | 99.4 | 95.1 | 96.0 | 83.4 | 57.4 | 97.4 | 76.3 | 52.7 | 70.1 |
| EuroSAT | 87.6 | 92.7 | 99.5 | 95.0 | 95.9 | 83.4 | 57.2 | 97.4 | 76.3 | 98.3 | 70.3 |
| CIFAR100 | 87.4 | 92.5 | 99.3 | 95.0 | 96.0 | 83.3 | 56.9 | 97.5 | 76.9 | 98.0 | 88.0 |
| Average | 88.0 | 92.4 | 91.9 | 93.9 | 87.4 | 75.2 | 39.2 | 92.0 | 52.8 | 60.9 | 76.9 |

Table 11: Accuracy of LoRA-FT, O-LoRA, CL-MoE, SEFE, KeepLoRA on the MLLM-DCL benchmark. Each row represents the performance on every dataset of the model trained after the corresponding task. Transfer, Average, and Last metrics are shown.

| (a) LoRA-FT | | | | | | | (b) O-LoRA | | | | | | |
|-------------|---------|---------|---------|---------|---------|------|------------|---------|---------|---------|---------|------|------|
| | Sensing | Medical | Driving | Science | Finance | | Sensing | Medical | Driving | Science | Finance | | |
| Transfer | 28.1 | 17.4 | 34.0 | 50.2 | 32.4 | | Transfer | 28.4 | 18.4 | 33.7 | 52.5 | 33.3 | |
| Sensing | 78.8 | 28.1 | 17.3 | 34.8 | 55.6 | | Sensing | 79.4 | 28.4 | 17.6 | 34.9 | 56.1 | |
| Medical | 75.5 | 58.4 | 17.5 | 32.7 | 54.8 | | Medical | 74.3 | 58.5 | 19.2 | 33.2 | 56.0 | |
| Driving | 70.0 | 47.5 | 52.3 | 34.6 | 40.9 | | Driving | 74.7 | 48.3 | 52.6 | 33.1 | 45.2 | |
| Science | 73.2 | 46.4 | 40.6 | 50.4 | 49.5 | | Science | 74.6 | 46.5 | 42.2 | 50.1 | 52.8 | |
| Finance | 69.3 | 44.3 | 29.1 | 41.4 | 88.4 | 54.5 | Finance | 72.3 | 46.9 | 31.6 | 41.5 | 88.1 | 56.1 |
| Average | 73.3 | 44.9 | 31.4 | 38.8 | 57.8 | 49.3 | Average | 75.0 | 45.7 | 32.6 | 38.5 | 59.6 | 50.3 |

| (c) CL-MoE | | | | | | | (d) SEFE | | | | | | |
|------------|---------|---------|---------|---------|---------|------|----------|---------|---------|---------|---------|------|------|
| | Sensing | Medical | Driving | Science | Finance | | Sensing | Medical | Driving | Science | Finance | | |
| Transfer | 28.3 | 19.4 | 34.1 | 48.6 | 32.6 | | Transfer | 28.1 | 19.6 | 33.9 | 52.4 | 33.5 | |
| Sensing | 79.4 | 28.3 | 18.7 | 35.2 | 56.4 | | Sensing | 78.8 | 28.1 | 18.6 | 35.1 | 56.2 | |
| Medical | 74.8 | 60.7 | 20.1 | 32.4 | 54.9 | | Medical | 77.1 | 59.5 | 20.7 | 33.0 | 55.7 | |
| Driving | 74.0 | 44.3 | 52.1 | 34.7 | 39.6 | | Driving | 77.8 | 51.6 | 52.5 | 33.5 | 47.4 | |
| Science | 71.0 | 47.4 | 40.0 | 50.7 | 43.3 | | Science | 77.9 | 48.4 | 44.7 | 50.4 | 50.1 | |
| Finance | 71.8 | 47.4 | 29.5 | 41.5 | 89.2 | 55.9 | Finance | 77.1 | 50.9 | 40.3 | 43.0 | 88.4 | 59.9 |
| Average | 74.2 | 45.6 | 32.1 | 38.9 | 56.7 | 49.5 | Average | 77.7 | 47.7 | 35.4 | 39.0 | 59.6 | 51.9 |

| (e) KeepLoRA | | | | | | |
|--------------|---------|---------|---------|---------|---------|------|
| | Sensing | Medical | Driving | Science | Finance | |
| Transfer | 28.5 | 16.6 | 34.1 | 55.6 | 33.7 | |
| Sensing | 80.0 | 28.5 | 17.0 | 35.1 | 55.1 | |
| Medical | 79.9 | 58.6 | 16.3 | 33.7 | 55.6 | |
| Driving | 79.8 | 57.7 | 53.1 | 33.7 | 54.6 | |
| Science | 79.2 | 54.9 | 51.1 | 51.6 | 57.2 | |
| Finance | 78.8 | 54.3 | 50.2 | 49.5 | 89.3 | 64.4 |
| Average | 79.6 | 50.8 | 37.5 | 40.7 | 62.4 | 54.2 |

Table 12: Accuracy of LoRA-FT, O-LoRA, CL-MoE, SEFE, KeepLoRA on the UCIT benchmark. Each row represents the performance on every dataset of the model trained after the corresponding task. Transfer, Average, and Last metrics are shown.

| (a) LoRA-FT | | | | | | | (b) O-LoRA | | | | | | |
|--------------|----------|---------|--------|--------|-------|-----------|------------|----------|---------|--------|--------|-------|-----------|
| | ImgNet-R | ArxivQA | VizWiz | IconQA | CLEVR | Flickr30k | | ImgNet-R | ArxivQA | VizWiz | IconQA | CLEVR | Flickr30k |
| Transfer | 52.6 | 18.3 | 6.0 | 17.0 | 40.3 | 26.8 | Transfer | 52.9 | 19.6 | 4.4 | 16.9 | 41.0 | 27.0 |
| ImgNet-R | 91.7 | 52.6 | 23.5 | 11.8 | 17.2 | 36.5 | ImgNet-R | 91.5 | 52.9 | 24.7 | 13.3 | 17.3 | 36.5 |
| ArxivQA | 90.5 | 92.1 | 13.1 | 2.1 | 14.2 | 21.5 | ArxivQA | 89.7 | 94.2 | 14.5 | 0.0 | 12.9 | 25.0 |
| VizWiz | 73.6 | 90.7 | 61.0 | 4.2 | 19.0 | 49.7 | VizWiz | 80.9 | 91.7 | 59.8 | 0.0 | 19.6 | 49.0 |
| IconQA | 72.7 | 77.1 | 53.7 | 79.7 | 17.4 | 47.8 | IconQA | 80.2 | 80.3 | 54.5 | 75.9 | 17.6 | 48.6 |
| CLEVR | 68.8 | 77.4 | 52.3 | 67.8 | 77.9 | 46.1 | CLEVR | 78.1 | 80.4 | 51.6 | 63.2 | 72.4 | 46.0 |
| Flickr30k | 58.6 | 76.7 | 45.7 | 67.4 | 61.6 | 58.0 | Flickr30k | 74.2 | 80.9 | 45.3 | 62.9 | 63.8 | 57.2 |
| Average | 76.0 | 77.8 | 41.6 | 38.8 | 34.6 | 43.3 | Average | 82.4 | 80.1 | 41.7 | 35.9 | 33.9 | 43.7 |
| | 52.0 | | | | | | | 53.0 | | | | | |
| (c) CL-MoE | | | | | | | (d) SEFE | | | | | | |
| | ImgNet-R | ArxivQA | VizWiz | IconQA | CLEVR | Flickr30k | | ImgNet-R | ArxivQA | VizWiz | IconQA | CLEVR | Flickr30k |
| Transfer | 52.0 | 19.3 | 7.4 | 17.8 | 41.3 | 27.6 | Transfer | 53.3 | 18.7 | 7.5 | 17.0 | 40.9 | 27.5 |
| ImgNet-R | 91.2 | 52.0 | 23.9 | 5.2 | 15.6 | 36.9 | ImgNet-R | 91.6 | 53.3 | 23.7 | 12.1 | 16.9 | 36.4 |
| ArxivQA | 89.2 | 92.5 | 14.8 | 10.0 | 15.7 | 26.2 | ArxivQA | 90.4 | 92.8 | 13.7 | 5.0 | 16.4 | 21.1 |
| VizWiz | 77.2 | 90.7 | 60.4 | 6.9 | 20.6 | 49.5 | VizWiz | 83.6 | 89.3 | 61.4 | 5.3 | 18.6 | 49.8 |
| IconQA | 79.5 | 76.2 | 51.0 | 54.7 | 19.4 | 47.9 | IconQA | 84.3 | 78.1 | 57.4 | 79.6 | 16.2 | 50.6 |
| CLEVR | 76.7 | 75.4 | 48.1 | 52.6 | 73.0 | 45.9 | CLEVR | 82.8 | 78.6 | 54.2 | 70.6 | 75.0 | 46.5 |
| Flickr30k | 61.2 | 75.8 | 44.4 | 52.6 | 54.4 | 57.3 | Flickr30k | 80.2 | 79.1 | 47.1 | 69.4 | 65.7 | 57.3 |
| Average | 80.2 | 77.1 | 40.4 | 30.3 | 33.1 | 44.0 | Average | 85.5 | 78.6 | 42.9 | 40.3 | 34.8 | 43.6 |
| | 50.9 | | | | | | | 54.3 | | | | | |
| (e) KeepLoRA | | | | | | | | | | | | | |
| | ImgNet-R | ArxivQA | VizWiz | IconQA | CLEVR | Flickr30k | | ImgNet-R | ArxivQA | VizWiz | IconQA | CLEVR | Flickr30k |
| Transfer | 52.8 | 20.4 | 9.2 | 18.1 | 41.5 | 28.4 | Transfer | 52.8 | 25.6 | 13.4 | 17.1 | 36.7 | |
| ImgNet-R | 91.5 | 52.8 | 25.6 | 13.4 | 17.1 | 36.7 | ImgNet-R | 91.5 | 52.8 | 25.6 | 13.4 | 17.1 | 36.7 |
| ArxivQA | 90.4 | 94.5 | 15.2 | 4.0 | 17.2 | 21.5 | ArxivQA | 90.4 | 94.5 | 15.2 | 4.0 | 17.2 | 21.5 |
| VizWiz | 85.5 | 92.4 | 61.5 | 10.1 | 21.0 | 50.6 | VizWiz | 85.5 | 92.4 | 61.5 | 10.1 | 21.0 | 50.6 |
| IconQA | 85.1 | 86.0 | 55.7 | 76.9 | 17.1 | 50.9 | IconQA | 85.1 | 86.0 | 55.7 | 76.9 | 17.1 | 50.9 |
| CLEVR | 84.1 | 89.3 | 51.5 | 68.3 | 72.6 | 47.8 | CLEVR | 84.1 | 89.3 | 51.5 | 68.3 | 72.6 | 47.8 |
| Flickr30k | 82.4 | 86.7 | 46.6 | 67.8 | 66.4 | 57.2 | Flickr30k | 82.4 | 86.7 | 46.6 | 67.8 | 66.4 | 57.2 |
| Average | 86.5 | 83.6 | 42.7 | 40.1 | 35.2 | 44.1 | Average | 86.5 | 83.6 | 42.7 | 40.1 | 35.2 | 44.1 |
| | 55.4 | | | | | | | 57.8 | | | | | |